FUNCTIONAL ANALYSIS OF RAD50 MUTANTS

FUNCTIONAL ANALYSIS OF RAD50 MUTANTS

By

SHUJIE XIAO, B.Sc.

A Thesis

Submitted to the School of Graduate Studies

in Partial Fulfilment of the Requirements

for the Degree

Master of Science

McMaster University

Master of Science(2007) McMaster University

(Biology) Hamilton, Ontario

TITLE: Functional Analysis of Rad50 Mutants

AUTHOR: Shujie Xiao, B.Sc.

SUPERVISOR: Dr. Xu-Dong Zhu

NUMBER OF PAGES: [x], 94

ABSTRACT

Mre11 and Rad50 form a complex with Nbs1 (MRN) in mammals and Xrs2 (MRX) in yeast. The MRN complex plays a role in many cellular processes, such as DNA damage sensing, DNA repair, cell cycle checkpoint and telomere maintenance. Rad50 contains a conserved ATP binding motif and its ATPase activity is essential for ATM activation *in vitro*. Using a tethering approach, I have shown that Rad50 can be targeted to telomeres through its fusion to hRap1. The fusion of hRap1 to Rad50 did not alter the property of Rad50. The fused wild-type Rad50 promoted telomerase-dependent telomere lengthening. However, the fusion proteins containing loss-of-function mutations in Rad50 (K42E and S1202R) did not. I have also shown that the fused wild-type Rad50 was able to form irradiation-induced foci in a manner similar to unfused Rad50. In contrast, the two defective mutants of Rad50 failed to accumulate irradiation-induced foci. Expression of the fusion proteins containing Rad50 mutants also interfered with the ability of endogenous Mre11 protein to form foci post irradiation. Thus our data suggest that the Rad50 mutants may function as dominant-negative alleles in cells.

ACKNOWLEGEMENTS

I would first like to thank my adviser Dr. Xu-Dong Zhu, who brought me in one of the most exciting fields of cell biology. During my stay at McMaster, she has taught me a great deal of techniques and how to be a good scientist. I am grateful to my committee members Dr. André Bédard and Dr. Juliet Daniel, for their useful advice. I would like to thank the old and new colleagues in the Zhu lab for their cooperation and friendships. I would also like to thank Dr. Yili Wu for her help and suggestions in doing experiments. I would like to thank my parents and husband for their encouragement and support. I would like to thank Dr. Turlough M. Finan and Dr. Elizabeth A. Weretilnyk for their help during my stay.

ABBREVIATIONS

ALT:	Alternative telomere lengthening
ATLD:	Ataxia-telangiectasia-like disorder
ATM:	Ataxia telangiectasia mutated
ATR:	ATM and Rad3 related
DDR:	DNA damage response
DNA-PKcs:	DNA-dependent protein kinase catalytic subunit
DSB:	DNA double-strand break
dsDNA:	Double-strand DNA
HR:	Homologous recombination
MRN:	Mre11/Rad50/Nbs1 complex
MRX:	Mre11/Rad50/Xrs2 complex
NBS:	Nijmegen breakage syndrome
NHEJ:	Non-homologous end joining
IF:	Immunofluorescence
IR:	Ionizing irradiation
IRIF:	Ionizing irradiation-induced foci
IP:	Co-immunoprecipitation
PD:	Population doubling
POT1:	Protection of telomeres protein 1
PIKK:	Phosphoinositide 3-kinase-related kinase
Rap1:	Repressor/Activator protein 1
RNAi:	RNA interference
ssDNA:	Single-strand DNA
TRF:	Telomere repeat binding factor

Table of Contents

List of Figures

Chapter 1

Introduction

Rad50 is the ATPase component of the Mre11/Rad50/Nbs1 (MRN) complex in mammals and the Mre11/Rad50/Xrs2 (MRX) complex in yeast. This complex is involved in many critical processes, such as DNA damage sensing, DNA damage repair, cell cycle checkpoint and telomere maintenance. Null mutations of any of the three components result in embryonic lethality in vertebrates. Mutations in Nbs1 and Mre11 give rise to Nijmegen breakage syndrome (NBS) and ataxia-telangiectasia-like disorder(ATLD), respectively. These diseases have been characterized by S-phase checkpoint failure, radiation sensitivity and chromosomal abnormality (D'Amours and Jackson 2002; Assenmacher and Hopfner 2004; Lisby and Rothstein 2004; Stracker *et al.* 2005; Lisby and Rothstein 2005; Slijepcevic and Al-Wahiby 2005; Su 2006). Patients having these diseases showed immunodeficiency, cancer predisposition, cerebeller development defects and increased radiosensitivity (Zhou *et al.* 2006). To date, no mutations in Rad50 have been found linked to genetic diseases in human (D'Amours and Jackson 2002).

1.1 Components and the structure of the Mre11/Rad50/-Nbs1 complex

1.1.1 Three components of the MRN complex

The MRN complex contains Mre11, Rad50 and Nbs1. Mre11 is a nuclease that possesses both 3'-5'exonuclease and ssDNA endonuclease activity. It contains five nuclease motifs at its N-terminus, which also contains a potential Nbs1 binding site. Mre11 also has DNA and Rad50 binding domains at the central region and C-terminus (Assenmacher and Hopfner 2004; D'Amours and Jackson 2002). Nbs1 serves as a mediator in the MRN complex. The N-terminus of Nbs1 contains the fork head associated (FHA) and breast cancer C-terminal (BRCT) domain. The Mre11 binding site locates near its C-terminus of Nbs1 (Kobayashi 2004). The very C-terminus of Nbs1 has been recently characterized as an ATM binding domain (Falck *et al.* 2005; You *et al.* 2005).

The ATPase Rad50 contains a conserved ATP binding cassette (ABC), which consists of Walker A, Walker B and signature motif. Walker A motif is located at N-terminus, whereas Walker B motif and signature motif are located at the C-terminus (Fig 1.1a). In the center of Rad50, there is a long coiled-coil repeat, which has a conserved Cys-X-X-Cys zinc hook in the middle. The signature motif and the Cys-X-X-Cys zinc hook form two interfaces between two Rad50 molecules. In the signature motif, binding of Ser793 side-chain Oγ in one Rad50 and Gly795 mainchain N in opposing Rad50 molecule to ATP γ-phosphate O promotes Rad50 dimerization (Hopfner and Tainer 2003; Moncalian *et al.* 2004). In addition, the Cys-X-X-Cys zinc hook coordinated by zinc ion can link MRN complexes through the long anti-parallel arms of Rad50. This structure has been observed by using atomic force and electron microscopy and believed to function in tethering DNA

ends and keep sister chromatids closer for DNA repair (Fig 1.1b) (Hopfner *et al.* 2000; Wiltzius *et al.* 2005).

1.1.2 Mutations of Rad50 related to the study

Although mutations in Rad50 have not been found in human yet, some mutations have been made to study the role of Rad50. Mutation in Rad50 signature motif, S1202R of human Rad50, is equivalent to Rad50 mutant S793R in *Pyrococcus furiosus*. S793R mutant prevents ATP-mediated dimerization of Rad50 and is analogous to a CFTR (cystic fibrosis transmembrane conductance regulator) mutation S549R, which is the cause of cystic fibrosis (Moncalian *et al.* 2004). Human S1202R mutant associates with wild-type Mre11/Nbs1 at a level comparable to wild-type Rad50 but is defective in ATP-dependent activity as well as the ability to activate ATM *in vitro* (Lee and Paull 2004; Lee and Paull 2005).

The yeast mutant Rad50 carrying K40E in the ABC catalytic domain, is capable of interacting with Mre11 but defective in ATP hydrolysis, DNA binding and unwinding *in vitro* (Paull and Gellert 1999). This mutant in yeast has been shown to be defective in DNA homologous recombination and non-homologous end joining (Chen *et al.* 2005).

Mutations outside of the conserved ATP binding cassette of Rad50 are defective in meiotic recombination in yeast perhaps due to its failure to release Spo11 (type II topoisomerase- like DNA transeterase) from DNA. These Rad50 mutants are called Rad50 S alleles. Constitutive DNA damage signal was detected in yeast carrying those Rad50 S alleles (Usui *et al.* 2001; Usui *et al.* 2006). However, the phenotypes in yeast can not be replicated in mice carrying the same mutants. The K22M of these mutants in mouse showed minimal cellular phenotype (insensitive to IR, hydroxyurea, etoposide or growth defect) but had profound impacts at organismal level. Mice carrying this mutation died

with metastatic thymic lymphoma several months after birth, suggesting that a chronic genotoxic stress has occurred (Bender *et al.* 2002). Furthermore, mice carrying this mutant can also bypass the ATM deficiency (Morales *et al.* 2005).

In this study, several human Rad50 mutants were made. K42E is a mutation in Walker A motif, which is equivalent to K40E in yeast. S1202R is a mutation in signature motif, whereas K22L is a mutation similar to K22M outside of Walker A motif.

1.2 Telomeres and the Mre11/Rad50/Nbs1 complex

1.2.1 Telomeres

Telomeres are specialized DNA-protein complexes located at the ends of linear chromosomes in eukaryotes. Human telomeric DNA consists of 2-30 kb dsDNA TTAGGG tandem repeats and G-rich ssDNA overhangs with about 150nt in length (de Lange 2002). The importance of telomeres lies in two aspects. Firstly, in human somatic cells, telomeres shorten every time cell divides. Shortened telomeres eventually lead to cell senescence, which is viewed as a tumor suppressor mechanism (Hanahan and Weinberg 2000). Most of cancer cells overcome telomere shortening by activating reverse transcriptase like enzyme, referred to as telomerase. Telomerase is responsible for adding telomere DNA repeats to chromosome ends, to maintain their telomere length. Some tumor cells do not activate telomerase and rely on a recombination dependent pathway termed alternative telomere lengthening (ALT) to maintain their telomere length (Wright and Shay 2000; Maser and Depinho 2002). Secondly, telomeres protect natural chromosome ends from being recognized as DNA damage sites. Protection of chromosome ends involves binding of telomeric proteins to telomere DNA and the formation of a specialized structure (Fig 1.2a). A large

duplex loop structure termed the t-loop has been proposed to protect telomeric DNA based on electron microscopy analysis of psoralen cross-linked telomeric DNA purified from human and mouse cells (Griffith *et al.* 1999; Stansel *et al.* 2001). The configuration of the t-loop appears to involve the invasion of the 3' overhang into the duplex telomere DNA. This structure could cap the chromosome ends and thus prevent telomeres from fusion or being processed by DNA damage repair proteins (de Lange and Petrini 2000).

1.2.2 Telomere associated proteins

Telomere associated proteins contribute to both telomere length control and telomere protection. These proteins are categorized into two groups: telomere specific proteins (also known as shelterin) and DNA repair proteins which are not specific to telomeres. Shelterin consists of six proteins: TRF1, TRF2, POT1, TIN2, TPP1 and hRap1 (de Lange 2005). TRF1 and TRF2 both have a conserved Myb domain at their C-termini, through which they specifically bind telomere dsDNA repeats. Both TRF1 and TRF2 form homodimers through their dimerization domains near their N-termini and do not interact with each other physically. (Zhong *et al.* 1992; Chong *et al.* 1995). *In vitro*, TRF2 is able to remodel artificial telomere DNA into loops, indicating that TRF2 plays a role in t-loop formation *in vivo* (Fig 1.2a) (Bianchi *et al.* 1997; Griffith *et al.* 1998; Bianchi *et al.* 1999; Griffith *et al.* 1999; Stansel *et al.* 2001). POT1 specifically binds to telomeric ssDNA (Lei *et al.* 2004; Loayza and de Lange 2004) and it is responsible for protection of 3' overhang (Hockemeyer *et al.* 2005; Yang *et al.* 2005). TIN2 and hRap1 were first identified as TRF1 and TRF2 interacting proteins respectively through a two-hybrid screen (Kim *et al.* 1999; Li *et al.* 2000). Recently it has been shown that TIN2 also links TRF2 and POT1 to TRF1 and thus works as a linchpin in shelterin (Liu *et al.* 2004; Ye *et al.* 2004). TPP1 is a TIN2 interacting

protein (Houghtaling *et al.* 2004; Liu *et al.* 2004; Ye *et al.* 2004). Shelterin also associates with DNA repair proteins such as the Mre11/Rad50/Nbs1 complex, WRN helicase, BLM helicase, XPF/ERCC1 endonuclease, DNA-PKcs, Rad51D, PARP-2 and Tankyrases. The precise role of DNA repair proteins at telomeres still remains elusive (de Lange 2005).

1.2.3 Dysfunctional telomeres

TRF2 is a telomere binding protein and plays an important role in telomere protection (van Steensel *et al.* 1998). Dysfunctional telomeres can be induced by expressing dominant negative alleles of TRF2. TRF2$^{\Delta B \Delta M}$, which lacks the N terminal basic domain and C-terminal Myb domain of TRF2, could strip endogenous TRF2 off telomeres, leading to telomere unprotection. Telomere overhangs are degraded by XPF/ERCC1 and telomeres are fused together by non-homologous end joining factors. TRF2 inhibition activates p53 and pRb dependent cell cycle checkpoints, leading to growth arrest and senescence (van Steensel *et al.* 1998; de Lange 2002; Jacobs and de Lange 2005). Expressing another deletion allele of TRF2-TRF2$^{\Delta B}$ also induced cell cycle checkpoint, growth arrest and senescence. However, this allele induces telomere deletion rather than telomere fusion, giving rise to t-loop sized dsDNA circles (Wang *et al.* 2004). In both cases, DNA damage repair factors will recognize dysfunctional telomeres and accumulate at telomeres (Takai *et al.* 2003).

1.2.4 Telomere length regulation

The elongation of telomere length is fulfilled by telomerase in eukaryotes (Greider and Blackburn 1985; Greider and Blackburn 1987). Telomerase is a reverse transcriptase,

which is expressed in germline cell and most of tumor cells but is not detectable in most normal somatic cells. The telomerase holoenzyme contains a highly conserved reverse transcriptase (TERT) and template RNA component together with other accessory proteins (de Lange 2006). Telomerase can add DNA repeats to the 3'overhang and the subsequent synthesis of the C-strand would create double-strand telomere DNA (Price 1997). The transcription of TERT is regulated by many genes such as Menin, the Mad/Myc pathway, and the TGFβ target Sip1, whereas production of RNA component is ubiquitous (Ducrest *et al.* 2002). The access of telomerase to telomeres is cell cycle regulated in yeast (Taggart *et al.* 2002; Smith *et al.* 2003). It has been proposed that telomere binding proteins are involved in telomere length control by regulating the access of telomerase to DNA end (Smogorzewska and de Lange 2004).

In budding yeast, the repressor/activator protein1-Rap1 is the major negative regulator of telomerase. Yeast Rap1 binds directly to telomere DNA and interacts with two Rap1 interaction factor: Rif1 and Rif2. Overexpression and mutagenesis studies confirmed Rap1 as a negative regulator of telomere length control (Shore 1994). The telomere ssDNA binding protein Cdc13 is also found to play an important role in telomerase dependent telomere length control and it is thought to recruit telomerase by interacting with telomerase accessory proteins (de Lange 2004).

In humans, shelterin and other telomere binding proteins are involved in telomere length regulation. Shelterin components are known to be cis-regulator of telomere length (Fig 1.2b) (de Lange 2005). TRF1 is a well-characterized negative regulator of telomerase-dependent telomere lengthening (van Steensel and de Lange 1997; Smogorzewska *et al.* 2000). TRF1, along with its partners TIN2 and tankyrase, functions in a negative feedback loop in telomere length control (de Lange 2004). Like TRF1, the overexpression of TRF2 also causes telomere shortening (Smogorzewska *et al.* 2000). The loss of POT1 leads to

very long telomeres, indicating loss of telomere length control (Loayza and de Lange 2003). In addition to shelterin components, DNA repair proteins are also found participating in telomere length regulation and protection (Slijepcevic and Al-Wahiby 2005).

1.2.5 MRN and telomeres

The MRN complex is implicated in telomere length control in mammals, plants, and yeast (Boulton and Jackson 1998; d'Adda di Fagagna *et al.* 2001; D'Amours and Jackson 2002). There are at least two pathways of telomere maintenance: telomerase-dependent and alternative telomere lengthening (ALT) pathways that is recombination dependent. The MRN complex is indicated to function in both pathways. In yeast, MRX complex is thought to generate ssDNA at chromosome ends that provide the access for telomerase to elongate telomeres (Kironmai and Muniyappa 1997; Nugent *et al.* 1998). MRX has also been shown to be critical to survivors in telomerase negative strains, which use homologous recombination pathway to maintain their telomeres (Le *et al.* 1999; Gallego and White 2001). In mammalian cells, the hint of the function of MRN in telomere maintenance came from abnormal telomere shortening in primary human fibroblast NBS cell line that did not have functional Nbs1 protein. It has been shown that human MRN complex is associated with telomeres in a cell-cycle-dependent manner (Zhu *et al.* 2000). Introduction of both Nbs1 and telomerase catalytic domains into NBS cell rescues telomere shortening, suggesting a role of MRN in telomerase-dependent telomere maintenance (Ranganathan *et al.* 2001). Mutations or knockdown of Nbs1 also result in telomere instability (Bai and Murnane 2003; Zhang *et al.* 2005). Recent work revealed that MRN is also important for the generation of the G-overhangs in human cell lines (Chai *et al.* 2006) and MRN is required to form a protective structure after telomere replication (Verdun *et al.* 2005). MRN is also

implicated in telomere replication and maintenance in ALT cells (Wu *et al.* 2000; Jiang *et al.* 2005).

1.3 DNA repair and Mre11/Rad50/Nbs1 complex

1.3.1 DNA double-strand break repair

DNA double-strand break (DSB) is always a threat to genome integrity and it can be caused by ionizing irradiation, genome toxic chemicals as well as internal factors such as stalled replication forks. However, cells have developed an efficient system to respond to DNA damage. DNA damage response system (DDR) consists of damage sensor proteins, which can detect the DNA damage promptly and subsequently send signals to downstream factors. The signals are amplified and diversified by signal transducers including ATM and ATR (ATM and Rad3-related) (Tel1 and Mec1 in *Saccharomyces cerevisiae*), DNA-PKcs, members of PIKKs that phosphorylate their substrates on serine or threonine residues followed by glutamine (SQ/TQ motifs) (Shiloh 2003). The transducers finally phosphorylate various effectors which can activate cell cycle checkpoint, DNA damage repair, and cell apoptosis, such as p53, chk1, chk2, etc. There are also lots of mediator proteins participating in the process although their exact roles are not clear yet (Jackson 2002; Petrini and Stracker 2003).

There are two major pathways of DSB repair in mammalian cells: non-homologous end joining (NHEJ) and homologous recombination (HR) (Kanaar et al. 1998; Karran, 2000). In NHEJ, the DNA ends are processed, annealed and finally ligated. NHEJ often involves loss or alteration of genetic information. The major factors participating in NHEJ include Ku heterodimer, DNA-PKcs, Artemis, DNA ligase IV and XRCC4. Broken

DNA attracts Ku heterodimer which activates DNA-PKcs. DNA-PKcs together with DNA ligaseIV and XRCC4 repair broken DNA (Kanaar *et al.* 1998; Karran 2000). Although DNA-PKcs can phosphorylate p53, it is not the most essential kinase to activate p53 in DNA double-strand break (Jimenez *et al.* 1999).

Homologous recombination is preferentially adopted in late S/G2 phase with the presence of sister chromotids (Baumann and West 1998). HR maintains the integrity of genetic information better than NHEJ. HR includes strand invasion, branch migration and Holiday junction structure resolution. In HR, DNA ends are first resected and then a sister homologous dsDNA is invaded and used as a template for DNA synthesis. It is carried out by Rad52 epistasis group (Rad50-55, Rad57, Rad59), and the MRN complex (Karran 2000).

1.3.2 MRN and DSB repair

MRN has been shown to play an essential role in sensing, processing and repairing DSBs. The MRN complex may tether broken DNA ends in order to increase the concentration of local DSBs (Moreno-Herrero *et al.* 2005). Biochemical studies have indicated that MRN complex may promote ATM monomreization and autophosphorylation, leading to ATM activation in DDR (Lee and Paull 2005). It has been shown that the MRN complex is required for ATM mediated cell cycle checkpoint in many mammalian cell lines (Carson *et al.* 2003; Uziel *et al.* 2003; Horejsi *et al.* 2004). In addition to function upstream of ATM, Nbs1 itself is a substrate of ATM after ATM activation (Lim *et al.* 2000). Phosphorylation of Nbs1 is involved in some aspects of cell cycle checkpoint (Buscemi *et al.* 2001). This suggests that MRN is a sensor as well as a mediator of DSB repair (Fig 1.3). A model has been proposed by Stavridi and Halazonetis (2005) to address the role of MRN

in DNA double strand break induced cell response. They proposed that the MRN complex is recruited to DSB site through an unknown mechanism and it further activates and recruits ATM to DNA damage sites. Then MRN and ATM function in an amplification loop, which activates a bigger pool of ATM (Stavridi and Halazonetis 2005). The MRN complex is also involved in homologous recombination and non-homologous end joining that are two major pathways of DSB repair (Su 2006). In *Schizosaccharomyces cerevisiae*, The DNA unwinding and nuclease activity of MRN toward DNA ends renders MRN a possible candidate of processing broken DNA ends before homologous recombination (Paull and Gellert 1998; Paull and Gellert 1999). Studies in yeast also demonstrated that MRN functions in homologous recombination of DSB repair (Bressan *et al.* 1999). Although it is still under debate, there is evidence that MRN may have a role in non-homologous end joining pathway (Zhang and Paull 2005).

Figure 1.1: Components of the Mre11/Rad50/Nbs1 complex. a) Motifs of Mre11, Rad50, Nbs1 proteins. b) Model of a functional MRN complex bound to broken DNA ends. Mre11 binds DNA ends and interacts with a Rad50 molecule. Two Rad50 proteins interact with each other through zinc hook domain and this structure helps to tether broken DNA ends. How Nbs1 binds to Mre11 and Rad50 is not clear yet. Modified from van den Bosch *et al.* (2003).

a) Mre11

Phosphoesterase domain DNA binding DNA binding

Rad50

Walker A motif Coiled–coil domain Coiled–coil domain Walker B motif

CXXC motif

Nbs1

FHA BRCT Mre11 binding motif ATM binding motif

b)

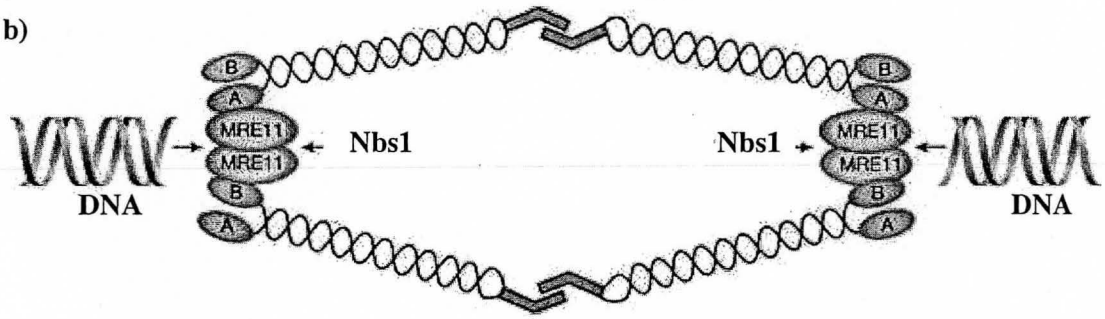

Figure 1.2: Telomere DNA and telomere binding proteins. a) t-loop structure of telomere DNA. A 3' overhang invades into duplex DNA, leading to the formation of a t-loop. Binding of TRF1 and TRF2 to telomere DNA facilitates t-loop formation. b) Shelterin complex on telomeres. Components of shelterin regulate telomere length in a cis-manner through inhibition of access of telomerase to telomere DNA. Modified from de Lange (2005).

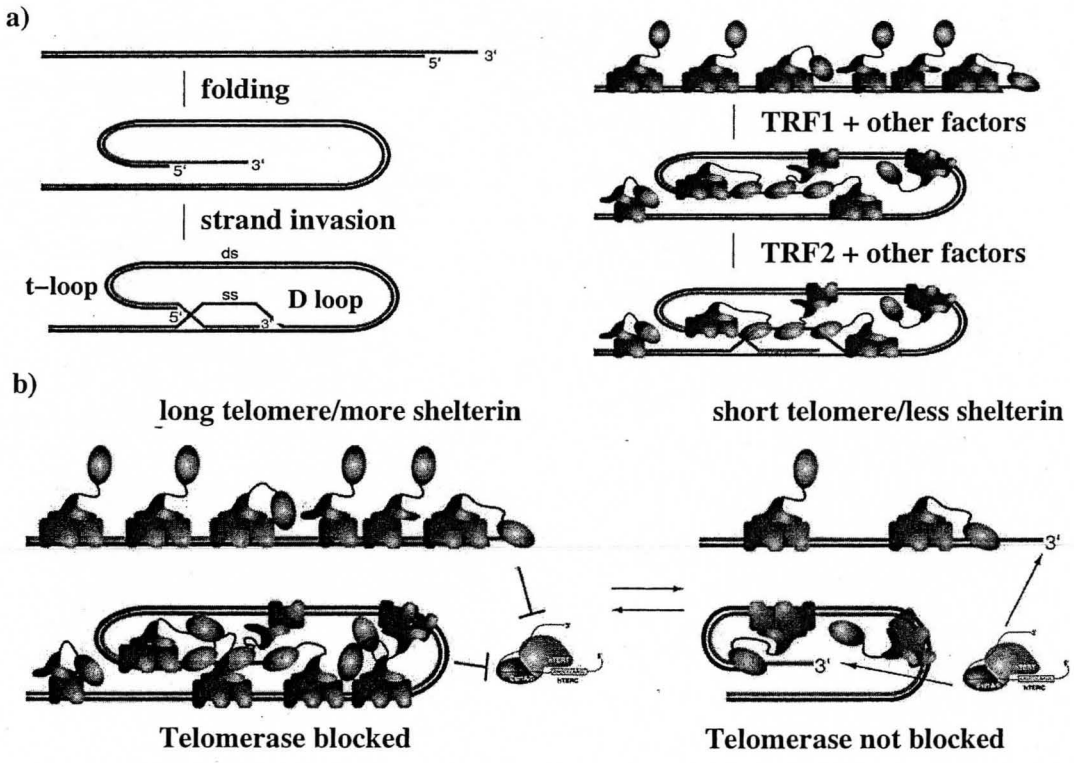
a)
5'
3'
folding
5'
3'
strand invasion
ds
t–loop
ss
D loop
5'
3'
TRF1 + other factors
TRF2 + other factors
b)
long telomere/more shelterin
short telomere/less shelterin
3'
3'
Telomerase blocked
Telomerase not blocked

Figure 1.3: Current model of DNA double-strand break repair. Modified from Zhou *et al.* (2006).

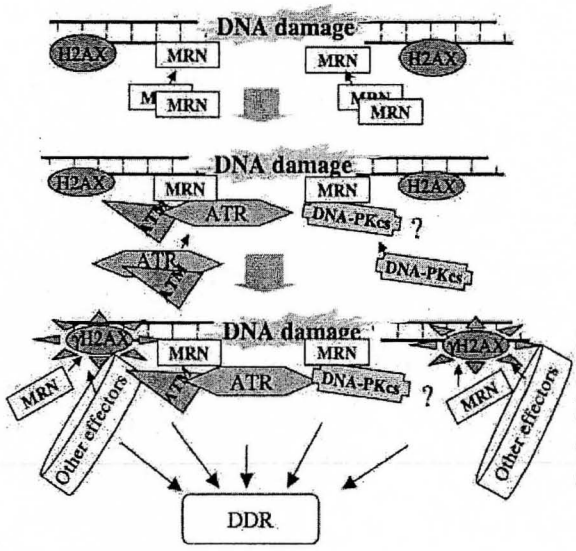

1st step: MRN detects DNA damage

2nd step: MRN recruits and activates PIKKs

3rd step: Activated PIKKs phosphorylate H2AX, leading to more MRNs and other DDR effectors recruited to the proximity of the DNA damage site to amplify DNA damage signaling and trigger DDR

Chapter 2

Materials and Methods

2.1 Construction of pLPCNmyc-hRap1-Rad50

Human Rap1 sequence was PCR amplified from pLPC-hRap1 plasmid. The hRap1 fragment and existing pLPCNmyc-hRad50 were digested with corresponding restriction enzyme and then ligated with T4 ligase. The final clone was verified by sequencing analysis.

2.2 Construction of pLPCNmyc-hRap1-Rad50 mutants

pLPCNmyc-hRap1-Rad50 plasmid was digested with BamH1 to yield a 1.2 kb hRap1 sequence. Existing pLPCNmyc-Rad50 K22L, pLPCNmyc-Rad50 K42E, pLPCNmyc-Rad50 S1202R were linearized with BamH1. Fragments were purified and ligated. The final clone was verified by sequencing analysis.

2.3 Alkaline Lysis Minipreparation of DNA

E. coli bacteria were shaken at 37°C overnight in 3 ml LB media made of 1% typtone, 0.5% yeast extract, 0.5% NaCl and 0.1 mg/ml ampicilin. Bacteria pellet was resuspended in 100μl solution 1 (50 mM glucose, 25 mM Tris-HCl pH 8.0, 10 mM EDTA pH 8.0). 200 μl solution 2 (0.2 M NaOH, 1%SDS) was added to lyse bacteria. After 5 minutes, 150 μl solution 3 (3.6 M potassium acetate, 14% glacial acetic acid) was added. 5 minutes later, samples were centrifuged at 13,000 rpm. Equal volume of phenol: chloroform (1: 1) was added to the supernatant. After vortexing and centrifugation, the aqueous layer was transferred to a new tube. DNA was ethanol precipitated, air-dried and then resuspended in 40 μl TE buffer (100 mM Tris and 10 mM EDTA, pH 8.0) with 0.02 μg/μl Rnase A. The concentration of DNA was approximately 0.2 μg/μl.

2.4 Transformation

1 μl DNA product from Alkaline Lysis Minipreparation was added to Top10 competent *E. coli* cells. Samples were incubated on ice for 30 minutes and then heat shock at 42°C for 45 seconds was performed. 1 ml LB without drug was added and mixed. Samples were incubated at 37°C for 1 hour. 50 μl supernatant was spread onto LB agar plate containing (100 μg/ml) ampicilin. The plates were incubated at 37°C for 16-18 hours.

2.5 Plasmid purification using QIAGEN plasmid Maxi kit

A single colony of *E. coli* was picked from LB agar selective plates and inoculated into 200 ml liquid LB containing 0.1 mg/ml ampicilin. After incubating at 37°C with vigorous

shaking for 16 hours, *E. coli* pellet was collected by centrifuging at 4200 rpm for 15 minutes. 10 ml buffer P1 (50 Mm Tris-HCl pH 8.0, 10 mM EDTA, 100 μg/ml Rnase A) was added to resuspend the pellet. Then 10 ml buffer P2 (0.2 M NaOH, 1%SDS) was added and samples were gently mixed and incubated at room temperature for 5 minutes. 10 ml chilled buffer P3 (3M potassium acetate pH 5.0) was added and samples were incubated on ice for 20 minutes. Samples were centrifuged at 13000 $\times g$ (4°C) for 30 minutes. Supernatant was applied to Qiagen column, which had been equilibrated with 10ml of buffer QBT (750 mM NaCl, 15% isopropanol, 50 mM MOPS pH 7.0, 0.15% Triton X-100). Then the column was washed 2 times with 30 ml buffer QC (1 M NaCl, 50 mM MOPS pH 7.0, 15% isopropanol). DNA was eluted with buffer QF (1.25 M NaCl, 50 mM Tris-HCl pH 8.5, 15% isopropanol). 10.5 ml isopropanol was added to precipitate DNA. After that samples were centrifuged at 13000 $\times g$ for 30 minutes at 4°C. DNA pellet was washed with 70% ethanol and air-dried. Then TE buffer was used to resuspend DNA.

2.6 Transfection of retroviral packaging phoenix cells

Phoenix is a helper free producer line for the generation of ecotropic and amphotropic retroviruses. It is based on the 293T cell line, which is a human embryonic kidney cells transformed with adenovirus E1a carrying T antigen. Phoenix cells were cultured at 37°C in DMEM containing 10% FBS, L-glutamine, streptomycin, penicillin and non-essential amino acid. Twenty four hours before transfection, 2.5 million phoenix cells were seeded onto 10 cm plate. 438 μl ddH_2O was used to resuspend 50 μg DNA. Then 62 μl 2M $CaCl_2$ was added. 500 μl 2$\times$ HBS (50 mM Hepes pH 7.05, 10 mM KCl, 12 mM dextrose, 280 mM NaCl, 1.5 mM Na_2HPO_4) was added drop by drop while mixture was bubbled. The mixture was added into the 10 cm cell culture plate. Cells were incubated at 37°C. 8-12

hours later, 9 ml of fresh media was changed. After incubating cells at 37°C for another 8-12 hours, 4 ml fresh media was changed. Virus-containing media was collected 8-12 hours later and filtered through 0.45 μm filter. Then 4 μl polybrene (4 μg/ml) was added and this virus-containing media was used immediately for infection.

2.7 Infection of recipient cell HT1080

HT1080 cells were cultured at 37°C in DMEM containing 10% BCS, L-Glutamine, streptomycin, penicillin and non-essential amino acid. A quarter million of HT1080 cells were seeded onto 10 cm plate 24 hours before infection. Then 4 ml of virus-containing media with 4 μl polybrene (4 μg/ml) was used to infect cells. After 8-12 hours, the same infection was performed. HT1080 cells were infected 5 times in total. Twelve hours after last infection, 9 ml fresh media was changed. Twelve hours later, 9 ml of media with 0.002 mg/ml puromycin was used for selection.

2.8 Protein extracts

Cells on a 10 cm plate were trypsinized and resuspended with media at a total volume of 10 ml. Cells were centrifuged at 1000 rpm at 4 °C for 5 minutes. The pellet was washed with cold 1× PBS. After centrifuging at 3000 rpm for 2 minutes, pellet was resuspend in buffer C (0.42 M KCl, 0.2% Nonidet P-40, 20 mM Hepes-KOH pH 7.9, 25% glycerol, 0.1 mM EDTA, 5 mM $MgCl_2$, 1 mM dithiothreitol (DTT), 1 μg/ml aprotinin, 1 μg/ml leupeptin, 1 μg/ml pepstatin and 0.5 mM phenylmethylsulfonyl fluoride (PMSF). The concentration of cells was about 200,000/μl. Mixture was incubated on ice for 30 minutes and then

centrifuged at 13,000 rpm for 10 minutes at 4°C. Supernatant was moved to a new tube and an equal volume of 2× laemmli buffer (100 mM Tris-HCl pH 6.8, 200 mM DTT, 3% SDS, 20% glycerol, 0.01% bromphenol blue) was added.

2.9 Western blotting

Protein extracts were boiled for 5 minutes and then separated by SDS-polyacrylamide gel electrophoresis for 1.5 hours. Proteins in the gel were transferred onto nitrocellulose membrane for 1 h at 90V in transfer buffer (25mM Tris, 125mM glycine, 10% SDS, 20% methanol, ddH_2O). The membrane was incubated in blocking buffer (10% milk powder, 0.5% Tween-20 in 1× PBS) for 1h at room temperature. It was then rinsed with incubation buffer (0.1% milk powder, 0.1% Tween-20 in 1× PBS), followed by incubation with primary antibody diluted in incubation buffer overnight at 4°C. Then the membrane was washed for 3 times (10 minutes each time) with incubation buffer, followed by incubation with secondary antibody (anti-mouse or anti-rabbit) diluted at 1: 20,000 for 1 hour. Following the incubation, the membrane was washed 4 times in incubation buffer and 2 times in PBS. ECL was performed (Amersham Biosciences, ECL Western Blotting Detection Reagents).

2.10 Immunofluorescence

Cells were cultured for 24 hours until 70%-80% confluent on coverslips. Then coverslips were rinsed with 1× PBS and fixed with 3% paraformaldehyde and 2% sucrose in 1× PBS for 10 minutes. The fixed cells were washed with PBS for 2 times at 5 minutes

each time, followed by permeabilizing in Triton X-100 buffer (0.5% Triton X-100, 20 mM Hepes-KOH pH 7.9, 50 mM NaCl, 3 mM $MgCl_2$, 300 mM Sucrose) for 10 minutes. Coverslips were washed again with PBS for 2 times and stored in PBS with 0.02% sodium azide. Cells were blocked with PBG (0.2% cold water fish gelatin, 0.5% BSA in PBS) and incubated with primary antibody diluted in PBG for 2 hours at room temperature. Cells were washed with PBG for 3 times (5 minutes each) and then incubated with secondary antibody (conjugated donkey anti-mouse or anti-rabbit) for 1 hour. Cells were washed again and stained by DAPI (4', 6-diamino-2-phenylindole at 5 mg/ml) for 10 minutes. Following 2 times wash in PBS, coverslips were mounted on a slide in 20 μl embedding buffer (20 mg p-phenylene diamine in 2 ml 10× PBS, 18 ml glycerol added) and sealed. Images were taken by a Zeiss Axioplan 2 microscope with a Hammamatsu C4742-95 camera and processed in Openlab software.

2.11 γ-irradiation

Cells were irradiated in a ^{137}Cs source (Cammacell 1000) at a dose of 12 Gy and fixed at indicated time post irradiation.

2.12 Immunoprecipitation

Cells harvested from 2× 25 cm confluent plates were resuspended in buffer C (5 times volume). After incubated on ice for 30 minutes. Cell extracts were spun at 13,000 rpm for 10 minutes. Supernatant was dialyzed against 50 times volume of buffer D (20 mM Hepes-KOH pH 7.9, 100 mM KCl, 25% glycerol, 0.1 mM EDTA (cold), 1 mM DTT and 0.5 mM

PMSF) at 4°C overnight. Extracts were centrifuged at 3000 rpm at 4°C for 5 minutes. Supernatant was transferred to a new tube and aliquoted for measuring protein concentration. Immunoprecipitation was performed using 500 μg protein extracts that were precleared with 1 μl (1:200 dilution) of mouse prebleed serum at 4°C for 1 hour. For IP, 1 μl primary anti-Myc was added and incubated at 4°C overnight (shaking). Following overnight incubation, 50 μl pre-blocked G beads was added to the extract and the mixture was incubated at 4°C with gentle shaking for 2 hours. Samples were centrifuged at 3000 rpm for 2 minutes and the supernatant was saved. IP Pellets were washed 5 times in buffer D containing 0.2% NP-40, 300 mM KCL, 1 mM DTT, 0.5 mM PMSF. Beads were resuspended in 50 μl laemmili buffer and boiled for 5 minutes. Supernatant was collected by centrifugation at 3000 rpm for 2 minutes and transferred to a fresh tube. Half of the resuspension was used for Western. Fifty microgram of protein extracts was used as input.

2.13 Isolation of genomic DNA

The cells were cultured over 3 months and harvested periodly. Cell pellets were washed once with cold PBS and stored at -80°C. Cell pellets were thawed on ice and resuspended with 1ml TNE (10 mM Tris pH 7.4, 100 mM NaCl, 10 mM EDTA) and then mixed with 1 ml TENS (TNE, 1% SDS). Following the incubation at 37°C overnight, 2 ml phenol/chloroform was added into each tube and mixed by inverting. Samples were centrifuged at 3000 rpm for 10 min. The aqueous phase was transfered to a new phase lock tube followed by another treatment with phenol/chloroform. Then the aqueous phase was transfered to a 15 ml tube containing 2 ml iso-propanol and 0.22 ml 2 M NaAc. After inverting for several times, genomic DNA was fished out and dissolved in a buffer containing 0.3 ml TNE and 100 μg/ml RNase A. Following incubation at 37°C for 0.5 h,

genomic DNA was mixed with blunt tips and then incubated for another 2 h. DNA was treated with TENS/ProtK (TNES, 100 μg/ml proteinaseK) at 37°C for 1 h. Following phenol/chloroform extraction, genomic DNA was transferred to eppendorf tubes containing 0.6 ml iso-propanol and 66 μl 2 M NaAc. After inverting, genomic DNA was fished out and dissolved in a buffer containing 200 μl $T_{10}E_{0.1}$ (10mM Tris-HCl pH 8.0, 0.1mM EDTA). DNA were incubated at 37°C for 0.5 h and at 4°C overnight and then stored at -20°C.

2.14 Digestion of genomic DNA

15 μl genomic DNA was mixed with 2.5 μl RsaI, 2.5 μl HinfI, 0.02 μl RNaseA, 70 μl ddH_2O and 10 μl 10× NEB buffer. Samples were mixed and incubated at 37°C for 16h.

2.15 Southern blotting

Digested DNA was separated in 0.7% agarose gel until the 1 kb marker was near the bottom. Three microgram digested DNA was loaded per lane. The gel was treated with 0.25 M HCl for 0.5 h and denatured in denaturation buffer (1.5 M NaCl, 0.5 M NaOH) for 1 hour, followed by neutralization buffer (3 M NaCl, 0.5 M Tris-HCl, pH 7.0) for another hour. The DNA was transferred to Hybond-N membrane. Following cross-linking and rinsing in ddH_2O, the membrane was put into churchmix buffer (0.5 M NaPi pH 7.2, 1 mM EDTA pH 8.0, 7% SDS, 1% BSA) and incubated at 65°C for 1h. Then the telomere DNA-containing probe was added and the membrane was incubated at 65°C overnight. The next day, the membrane was washed using churchwash (40 mM NaPi pH 7.2, 1 mM EDTA pH 8.0, 1% SDS) for 3 times and then exposed to PhosphorImage screen. The blot was analyzed as

described (Karlseder *et al.* 2002).

2.16 Growth curve

HT1080 cell lines were seeded on 24 well plate in triplicate. A total of 250 cells were seeded in each well at the 4th day of selection. Cells were split 1:16 to 1:8 when they got confluent. Number of cells in each well was counted every day for 19 days. Relative cell numbers (average cell number in each well $\times$ split ratio) were plotted over time.

2.17 Antibodies

Anti-Rad50, anti-Mre11, anti-hRap1 (#765), anti-TRF2 (#647), anti-TRF1 (#371) were gifts from Dr. Titia de Lange. Anti-Myc (9E10) was from Oncogene Biosciences. Anti-γ-tubulin was from Sigma. Anti-γ-H2AX and anti-H2AX were from Upstate Biotechnology. Anti-mouse and anti-rabbit secondary antibodies were purchased from Jackson Laboratories.

Chapter 3

Results

3.1 Rad50 promoted telomere lengthening

pLPCNmyc-Rad50 S1202R, together with the previously-made constructs pLPCNmyc, pLPCNmyc-Rad50, pLPCNmyc-Rad50 K22L, pLPCNmyc-Rad50 G41D, pLPCNmyc-Rad-50 K42E, pLPCNmyc-Rad50 R83I were used in the study. These constructs were introduced into human fibrosarcoma HT1080 cell lines. All of the expressed proteins have Myc tag at their N-termini.

3.1.1 Rad50 mutants expressed predominantly in cytoplasm

Immunofluorescence (IF) was conducted by using mouse anti-Myc antibody to investigate the expression pattern of Rad50 proteins (Figure 3.1a). pLPCNmyc-Rad50 and pLPCNmyc-Rad50 K22L were mainly in nucleus but all remaining mutants were outside of nucleus several days after infection. Western analysis using anti-Myc antibody showed that all mu-

tants except for R83I, had similar expression level with wild-type Rad50. (Figure 3.1b). These results indicate that expression of Rad50 mutants are predominantly in cytoplasm.

Because K22L mutant is the only mutant that can be expressed in nucleus, I did several experiments to investigate the response of K22L mutant to DSB repair and stalled replication forks. Ionizing irradiation (causing DSB) and HU (causing stalled replication fork) treated DNA damage assays were performed in pLPCNmyc-Rad50 and pLPCNmyc-Rad50 K22L expressing cell lines. However, no significant difference between these two cell lines was found in terms of foci formation after treatment with IR and HU (data not shown). The reported K22M mutant is thought to be a gain-of-function mutation and no difference was detected at the cellular level in cell lines expressing K22M (Bender *et al.* 2002). It might be possible that K22L may behave like K22M. Our data suggest that K22L may also be associated with a gain-of-function.

3.1.2 Fusing hRap1 to Rad50

The fact that defective Rad50 mutants predominantly accumulate in the cytoplasm made it difficult to study the function of these Rad50 mutants in cells. To overcome this problem, the Rad50 proteins were fused to a telomere protein. The fusion was able to target Rad50 mutants into nucleus, especially to telomeres.

The reason of choosing hRap1 in the study lied in several aspects. First of all, hRap1 is a telomere specific protein, which interacts with TRF2 and MRN in human. Fusing hRap1 to Rad50 proteins may target the Rad50 mutants into nucleus, especially to telomeres. Given the fact that only 5% of endogenous Rad50 protein is associated with telomeres. Furthermore, overexpression of hRap1 only caused slightly telomere elongation (Li *et al.* 2000; Li and de Lange 2003), which would only have slight effects on the analysis

on telomere length. Thus hRap1 was considered as a good candidate for fusion.

hRap1 was directly fused to the N-terminus of Rad50 to generate a fusion protein (Figure 3.2). Several constructs were made and they are pLPCNmyc, pLPCNmyc-hRap1, pLPCNmyc-Rad50, pLPCNmyc-hRap1-Rad50, pLPCNmyc-hRap1-Rad50 K22L, pLPCNmyc-hRap1-Rad50 G41D, pLPCNmyc-hRap1-Rad50 K42E, pLPCNmyc-hRap1-Rad50 R83I, pLPCNmyc-hRap1-Rad50 S1202R. These constructs were used in retrovirus infection to generate stable HT1080 cell lines.

3.1.3 Property of hRap1-Rad50 proteins

Western analysis showed the expression of the fusion proteins

HT1080 cells expressing pLPCNmyc, pLPCNmyc-hRap1, pLPCNmyc-Rad50, pLPCNmyc-hRap1-Rad50, pLPCNmyc-hRap1-Rad50 K22L, pLPCNmyc-hRap1-Rad50 K42E, pLPCNmyc-hRap1-Rad50 S1202R were harvested and the lysates were used for western blotting. As shown in Figure 3.3, the fusion proteins with a molecular weight of 210 kDa were detected by anti-Myc, anti-Rad50 and anti-hRap1 antibodies. These results suggest that the full-length fusion proteins were expressed. As a control, anti-Rad50 and anti-hRap1 antibodies also detected endogenous Rad50 and hRap1, respectively. Consistent with previously-published data (Li *et al.* 2000; Li and de Lange 2003), the expression of Myc-hRap1 is at least 5 folds higher than endogenous hRap1. Expression of Myc-Rad50 is similar to endogenous Rad50. The expression of all fusion proteins is also similar to that of endogenous Rad50. These data indicate that the expression of fusion Rad50 is at a physiological level of Rad50.

The fusion proteins are associated with telomeres

Immunofluorescence using anti-Myc antibody was conducted. As shown in figure 3.4, the expression levels of fusion proteins were consistent with the western blotting (Figure 3.3). Further more, the Myc-hRap1-Rad50 proteins were located in the nucleus. This suggested that hRap1 brought Rad50 mutants into nucleus.

Since the nucleoplasmic proteins obscured the telomere foci, IF using extraction method, which removed the nucleoplasmic proteins, was conducted. The coverslips were co-stained with anti-Myc and anti-TRF1 antibodies (Figure 3.5). TRF1, the telomere repeat binding factor 1, was used as marker of telomeres. The results showed that the TRF1 foci co-localized with Myc containing foci quite well in fusion proteins expressing cells, indicating that the fusion proteins localized to telomeres. In addition, the co-localization of TRF1 foci and Myc-hRap1-Rad50 foci was better than that of unfused Rad50 foci, suggesting that by fusing to hRap1, the amount of fusion proteins on telomeres were higher than unfused Rad50.

hRap1-fused Rad50 interacts with endogenous Mre11 and hRap1

To examine the interaction between expressed proteins and other proteins, co-immunoprecipitation using anti-Myc antibody was conducted. As shown in Figure 3.6, the hRap1 fused Rad50 proteins interacted with Mre11 at a level similar to that of the unfused Rad50. However, hRap1 did not interact with Mre11 directly, suggesting that the fusion proteins interact with Mre11 through the Rad50 portion of the fusion protein. Western analysis using anti-TRF2 antibody showed that all the fusion proteins interacted with TRF2. Expressed Myc-hRap1 also interacted with TRF2. These results suggest that the fusion proteins interact with TRF2 through its hRap1 part. In addition, all of the expressed proteins did not

interact with TRF1 directly as expected. Figure 3.6 also shows that all the proteins were detected by anti-Myc antibody.

The expression levels of endogenous telomere binding proteins were also examined. The expression of TRF1, TRF2 and POT1 were not affected by expression of the fusion Rad50 alleles in cells (Figure 3.7).

Taken together, hRap1 fused Rad50 proteins interact with its partner Mre11 and TRF2. Fusion of hRap1 targets Rad50 to telomeres.

hRap1-fused wild-type Rad50 promotes telomere elongation but not defective Rad50 mutants

Human fibroblastoma HT1080 cell lines expressing vector, Myc-hRap1, Myc-Rad50, Myc-hRap1-Rad50, Myc-hRap1-Rad50 K22L, Myc-hRap1-Rad50 K42E, Myc-hRap1-Rad50 S1202R were cultured for about 150 population doublings (PD). Genomic DNA and protein extracts were collected at various PDs.

Expression level of proteins were confirmed by western analysis (Figure 3.8). Except for Myc-hRap1-Rad50 K22L, the expression levels of other proteins remain similar throughout cell culturing. Expression of Myc-hRap1-Rad50 K22L decreased after 100 PD.

To investigate telomere length dynamics, southern blotting was conducted by using $^{*}P^{32}$-labeled telomere probe (Figure 3.9). Median telomere length was measured by using ImageQuant software. From about PD10 to PD150, telomere length in cells expressing vector control and Rad50 showed little change. In the Myc-hRap1 expressing cell line, there was a slight lengthening of telomeres. Myc-hRap1-Rad50 expressing cell line displayed a continuous telomere lengthening pattern (about 20 bp/PD) (Figure 3.9), while Myc-hRap1-

Rad50 K22L expressing cell line showed a plateau pattern after 100 PD which may be due to the drop of protein expression (data not shown). In two of the deficient mutants Myc-hRap1-Rad50 K42E and Myc-hRap1-Rad50 S1202R, the lengthening of telomere was not observed. The Myc-hRap1-Rad50 K42E expressing cell line even showed a slight telomere shortening (about 4 bp/PD).

3.2 The function of Rad50 in DSB repair

3.2.1 hRap1-fused wild-type Rad50 is able to form irradiation-induced foci in response to ionizing irradiation

It has been well demonstrated that the MRN complex can form DSB induced foci in various kinds of cells (Mirzoeva and Petrini 2001). Ionizing irradiation-induced foci (IRIF) has been widely used to examine the response of MRN to DSB. IRIF can be seen by IF using antibodies against the protein of interest. The percentage of IRIF positive cells, number of foci per cell, the shape and the size of the foci are dependent upon the protein of interest, radiation dose, incubation time after IR as well as cell type (Mirzoeva and Petrini 2001).

HT1080 cells expressing pLPCNmyc, pLPCNmyc-hRap1, pLPCNmyc-Rad50, pLPCNmyc-hRap1-Rad50, pLPCNmyc-hRap1-Rad50 K22L, pLPCNmyc-hRap1-Rad50 K42E, pLPCNmyc-hRap1-Rad50 S1202R were treated with 12 Gy ionizing irradiation. It has been shown that MRN form IRIF several hours post irradiation (Mirzoeva and Petrini 2001). Cells were fixed 4, 8, or 22 hours after irradiation and used for IF. Unlike the telomere foci, the IRIF were shown to be influenced by extraction, thus the method without extraction of nucleoplasmic protein was used in this study. Myc-hRap1 showed a homo-

geneous Myc staining pattern post irradiation. Cells having more than five IRIFs were scored positive. As shown in Figure 3.11a and Figure 3.13a, the percentage of IRIF positive cells in Rad50, Myc-hRap1-Rad50 and Myc-hRap1-Rad50 K22L expressing cell lines were similar (about 40%). But the mutants K42E (about 2%) and S1202R (about 10%) are defective in forming IRIF at 8 hours after irradiation. In addition, these Rad50 IRIFs co-localized with endogenous Mre11 (Figure 3.11a). Mre11 is used as a marker of IRIF site.

IF was also conducted at 4 hours and 22 hours post irradiation (Figure 3.11b). The percentage of Rad50 IRIF positive cells was scored (Figures 3.13b and 3.13c). The data indicated that at these two time points, the formation of Rad50 IRIF in the two defective mutants were still low compared to Myc-hRap1-Rad50 expressing cell line.

3.2.2 The ability of endogenous Mre11 to form IRIF is defective in cells expressing defective Rad50 mutants

To examine whether these two defective mutants function as dominant negative alleles, IF was conducted to examine the IRIF of endogenous Mre11 by using anti-Mre11 antibody. As shown in Figure 3.12 and Figure 3.13d, in Myc-Rad50, Myc-hRap1-Rad50 and Myc-hRap1-Rad50 K22L expressing cell lines, the formation of Mre11 foci was not affected compared to vector control cell line (about 30%). However, in the two defective mutants expressing cell lines, the endogenous Mre11 foci formation decreased to about 7% and 10%. It suggested that the mutants K42E and S1202R also block the endogenous Mre11 in forming IRIF and thus may function as partially dominant negative alleles.

3.2.3 The role of Rad50 in sensing uncapped telomere

Uncapped telomeres can be induced by expressing a dominant negative allele-TRF2$^{\Delta B\Delta M}$ that lacks the N-terminus basic domain and C terminal Myb domain of TRF2. This allele itself did not bind to telomeres and it also affected the accumulation of endogenous TRF2 on telomeres (van Steensel *et al.* 1998).

Because the MRN complex has been demonstrated as a DNA damage sensor (Moreno-Herrero *et al.* 2005), it is possible that it may also play a role in sensing uncapped telomeres which share the same checkpoint pathways as DNA double-strand break repair (de Lange 2002). pWZL vector and TRF2$^{\Delta B\Delta M}$ alleles were introduced into the HT1080 cell lines expressing vector, Myc-hRap1, Myc-Rad50, Myc-hRap1-Rad50, Myc-hRap1-Rad50 K22L, Myc-hRap1-Rad50 K42E, Myc-hRap1-Rad50 S1202R. Western blot was conducted to confirm the protein expression (Figure 3.14). Population growth over time were plotted (Figure 3.15). The results has been confirmed by another independent infection. Compared to the vector control cell lines, all of the TRF2$^{\Delta B\Delta M}$ expressing cell lines showed slower population doubling rate. The rate of growth in Myc-hRap1-Rad50 K42E/ TRF2$^{\Delta B\Delta M}$ and Myc-hRap1-Rad50 S1202R/TRF2$^{\Delta B\Delta M}$ expressing cell lines were similar to that in Myc-hRap1-Rad50/TRF2$^{\Delta B\Delta M}$ cell line. These results suggest expressing defective Rad50 mutants did not affect sensing of uncapped telomeres.

3.2.4 Expression of the fusion Rad50 mutants has no impact on the dynamics of phosphorylated γ-H2AX post irradiation

γ-H2AX is phosphorylated a few minutes after DSB occurs. phosphorylated γ-H2AX foci are established markers for DSB. phosphorylated γ-H2AX and the repair proteins

may enforce each other in forming IRIFs, although the initial recruitment of the repair proteins may not be dependent on phosphorylated γ-H2AX. It has been suggested that the presence of phosphorylated γ-H2AX is a reflection of the extent of DNA damage (Paull *et al.* 2001; Foster and Downs 2005; Stucki and Jackson 2006). In order to investigate the behavior of Rad50 mutants in response to DSB, the dynamic of phosphorylated γ-H2AX formation after irradiation was monitored by western blot (Figure 3.16). Post 12 Gy irradiation, cell extracts were made from HT1080 cell lines expressing different Rad50 alleles. Western blot was conducted by using anti-phosphorylated γ-H2AX antibody. In the vector control cell line, a gradually decrease pattern of phosphorylated γ-H2AX signal was observed, suggesting that the DSB were gradually repaired. In cell lines expressing unfused Rad50, fusion Rad50 as well as the two defective mutants, the pattern of phosphorylated γ-H2AX decrease remains the same. These results suggest that the mutants did not affect the dynamics of phosphorylated γ-H2AX. Total H2AX blot was used as a loading control.

Figure 3.1: Cytoplasmic expression of Myc-tagged Rad50 mutants. a) Immunofluorescence showing localization of non-fused Rad50 proteins in HT1080 cell line. Interphase HT1080 cells infected with Myc-tagged wild-type Rad50 and Rad50 mutants were fixed and stained with DAPI and anti-Myc (9E10) antibody. Wild-type Rad50 and Rad50 K22L are in the nucleus, whereas the other Rad50 mutants are all outside of nucleus. b) Western blotting showing the expression levels of Myc-tagged wild-type Rad50 and Rad50 mutants in HT1080 cells. Primary antibody used is indicated on the left side.

a)

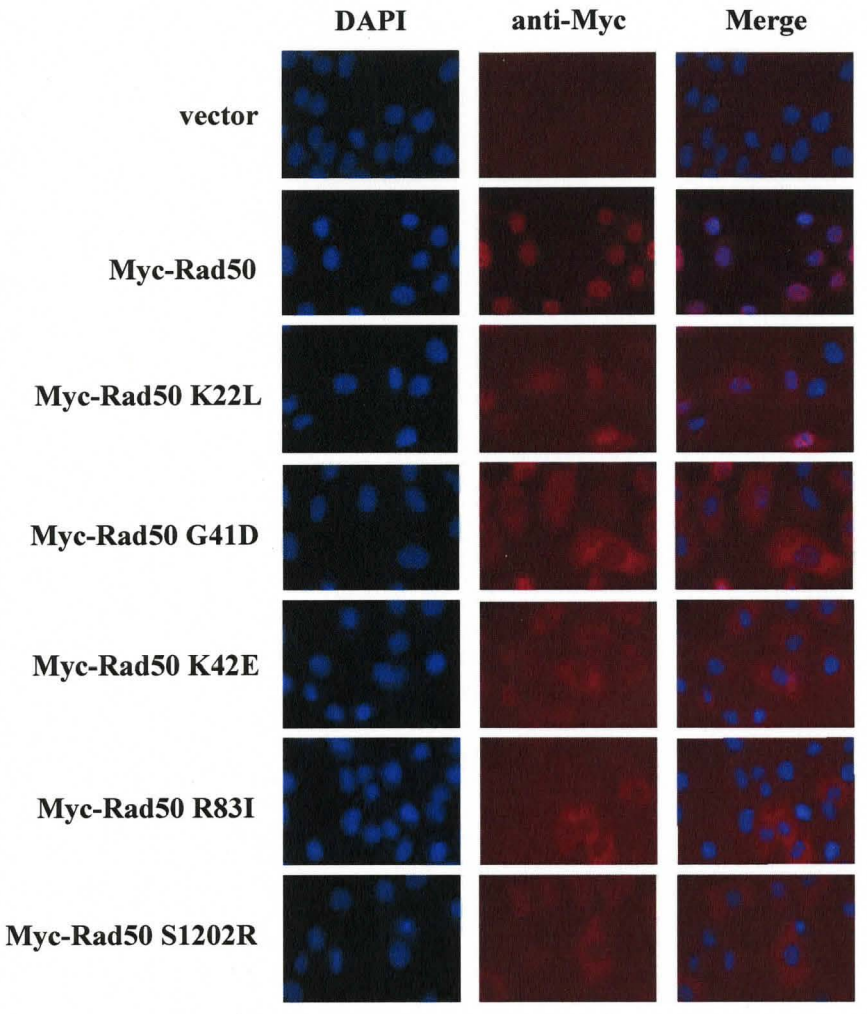
DAPI
anti-Myc
Merge
vector
Myc-Rad50
Myc-Rad50 K22L
Myc-Rad50 G41D
Myc-Rad50 K42E
Myc-Rad50 R83I
Myc-Rad50 S1202R

b)

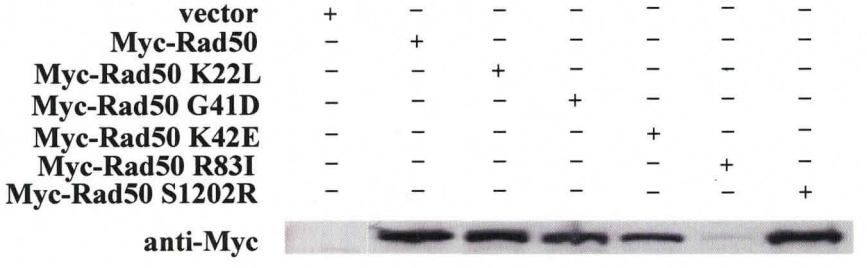
vector + − − − − − −
Myc-Rad50 − + − − − − −
Myc-Rad50 K22L − − + − − − −
Myc-Rad50 G41D − − − + − − −
Myc-Rad50 K42E − − − − + − −
Myc-Rad50 R83I − − − − − + −
Myc-Rad50 S1202R − − − − − − +
anti-Myc

Figure 3.2: Fusing hRap1 to Rad50. hRap1 was inserted between Myc-tag and Rad50 protein.

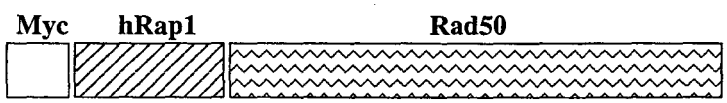

N–terminus

Figure 3.3: Expression of the hRap1-fused Rad50 proteins. Protein extracts from HT1080 cells infected with vector, Myc-hRap1, Myc-Rad50 and fusion proteins were used in western blotting. Primary antibodies used are indicated on the left side.

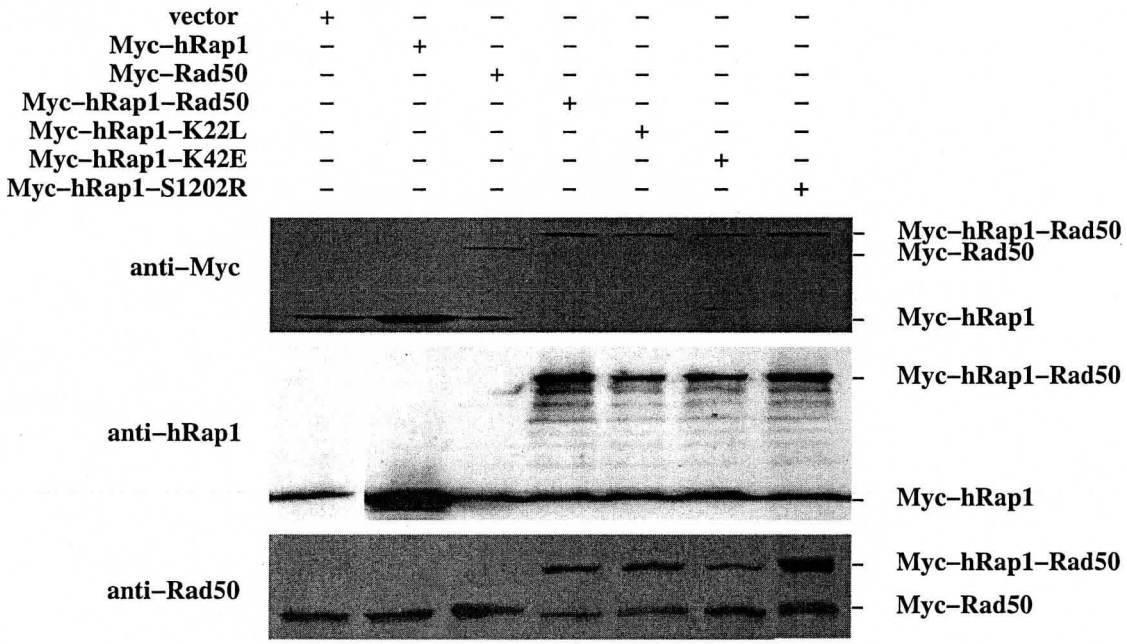
vector + – – – – – –
Myc–hRap1 – + – – – – –
Myc–Rad50 – – + – – – –
Myc–hRap1–Rad50 – – – + – – –
Myc–hRap1–K22L – – – – + – –
Myc–hRap1–K42E – – – – – + –
Myc–hRap1–S1202R – – – – – – +
anti–Myc
Myc–hRap1–Rad50
Myc–Rad50
Myc–hRap1
anti–hRap1
Myc–hRap1–Rad50
Myc–hRap1
anti–Rad50
Myc–hRap1–Rad50
Myc–Rad50

Figure 3.4: hRap1-fused Rad50 proteins are predominantly expressed in nucleus. Interphase HT1080 cells expressing vector, Myc-hRap1, Myc-Rad50 and fusion proteins were fixed. Immunofluorescence was conducted by staining cells with DAPI and anti-Myc antibody.

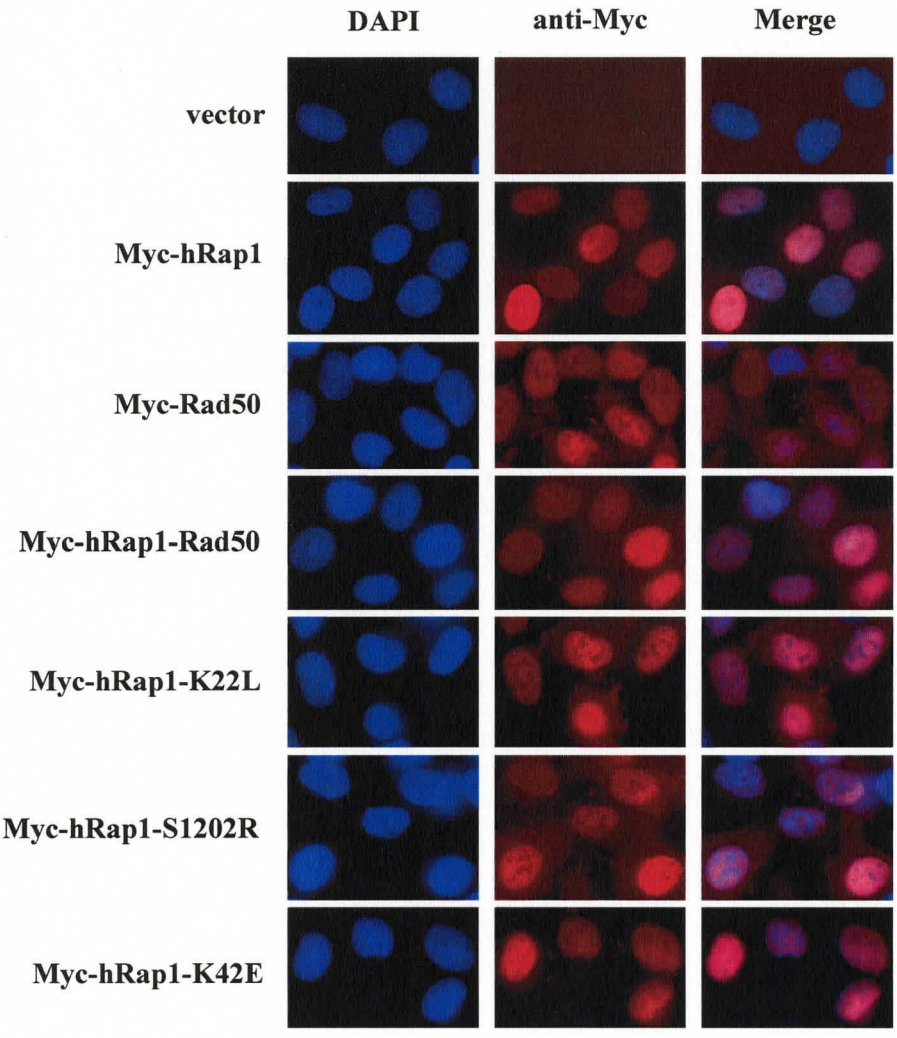
DAPI
anti-Myc
Merge
vector
Myc-hRap1
Myc-Rad50
Myc-hRap1-Rad50
Myc-hRap1-K22L
Myc-hRap1-S1202R
Myc-hRap1-K42E

Figure 3.5: Co-localization of hRap1-fused Rad50 proteins with TRF1. TRF1 was used as a marker of telomeres. Interphase HT1080 cells expressing various constructs were permeabilized with Triton-X 100 and stained with anti-Myc (9E10) (TRITC) in conjunction with anti-TRF1 (FITC) antibodies. Foci of fused Rad50 proteins co-localized with TRF1 foci, indicating that fusion to hRap1 targeted these proteins to telomeres.

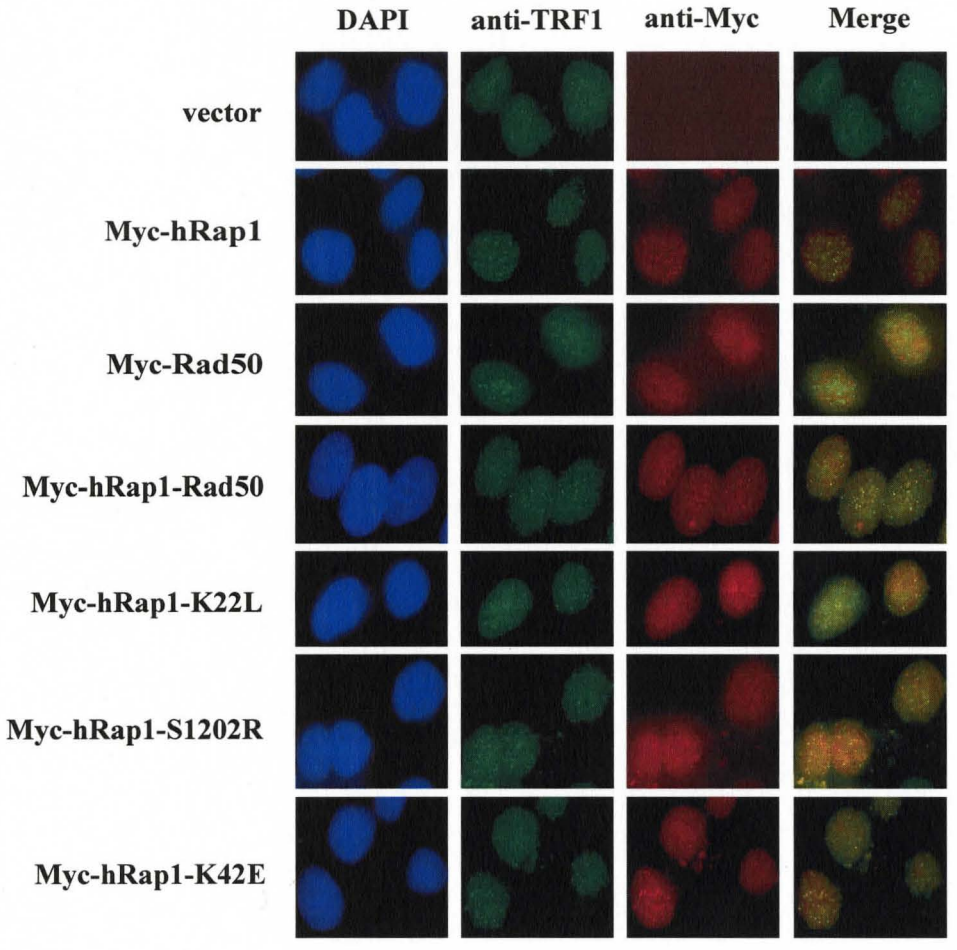
DAPI
anti-TRF1
anti-Myc
Merge
vector
Myc-hRap1
Myc-Rad50
Myc-hRap1-Rad50
Myc-hRap1-K22L
Myc-hRap1-S1202R
Myc-hRap1-K42E

Figure 3.6: hRap1-fused Rad50 proteins interact with Mre11 and TRF2. Whole cell extracts from HT1080 cells expressing vector, Myc-hRap1, Myc-Rad50 and fusion proteins were used in anti-Myc co-immunoprecipitation followed by western blotting. The immunoprecipitates and 20% of the input were used in western blotting. Primary antibodies used are indicated on the left side.

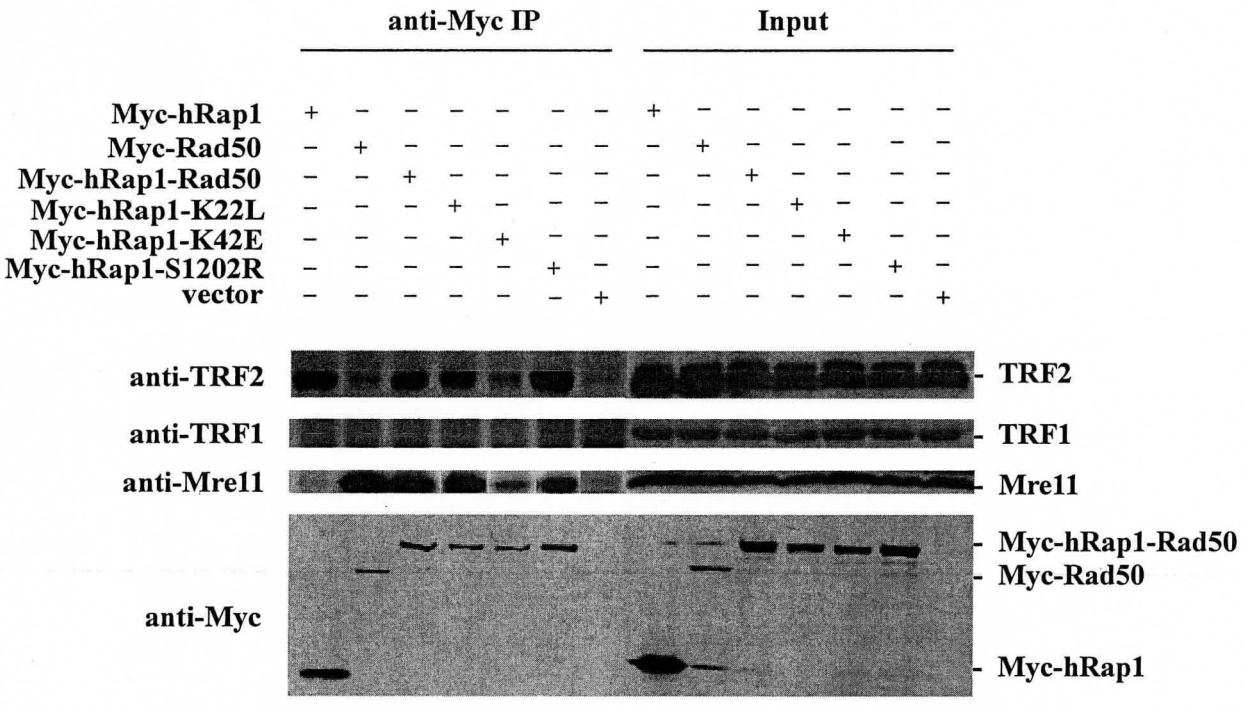
anti-Myc IP
Input
Myc-hRap1 + − − − − − − + − − − − − −
Myc-Rad50 − + − − − − − − + − − − − −
Myc-hRap1-Rad50 − − + − − − − − − + − − − −
Myc-hRap1-K22L − − − + − − − − − − + − − −
Myc-hRap1-K42E − − − − + − − − − − − + − −
Myc-hRap1-S1202R − − − − − + − − − − − − + −
vector − − − − − − + − − − − − − +
anti-TRF2
TRF2
anti-TRF1
TRF1
anti-Mre11
Mre11
anti-Myc
Myc-hRap1-Rad50
Myc-Rad50
Myc-hRap1

Figure 3.7: Expression of various fusion proteins does not affect the expression of TRF1, TRF2 and POT1 in HT1080 cells. Cell extracts from HT1080 cells expressing vector, Myc-hRap1, Myc-Rad50 and fusion proteins were used in western blotting. Primary antibodies used are indicated on the left side. γ-tubulin blot was used as a loading control.

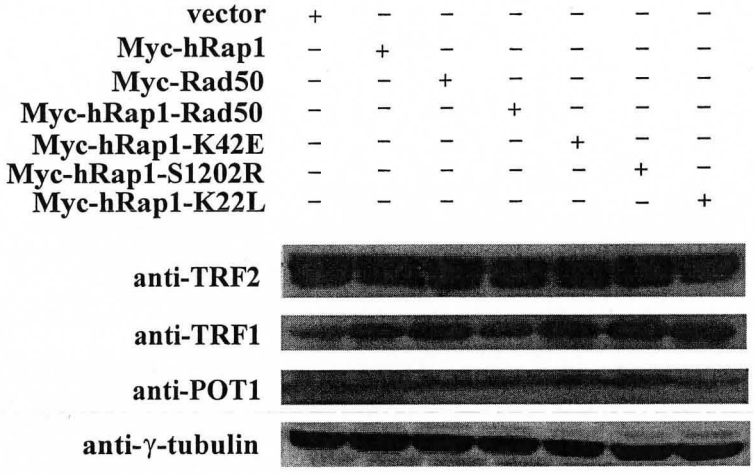
vector + − − − − − −
Myc-hRap1 − + − − − − −
Myc-Rad50 − − + − − − −
Myc-hRap1-Rad50 − − − + − − −
Myc-hRap1-K42E − − − − + − −
Myc-hRap1-S1202R − − − − − + −
Myc-hRap1-K22L − − − − − − +
anti-TRF2
anti-TRF1
anti-POT1
anti-γ-tubulin

Figure 3.8: Expression of hRap1-fused Rad50 proteins in the long-term culturing HT1080 cell lines. Cell extracts from HT1080 cells expressing vector, Myc-hRap1, Myc-Rad50 and fusion proteins were harvested at indicated population doublings during cell culture. Western blotting was conducted by using anti-Myc antibody. γ-tubulin blot was used as a loading control.

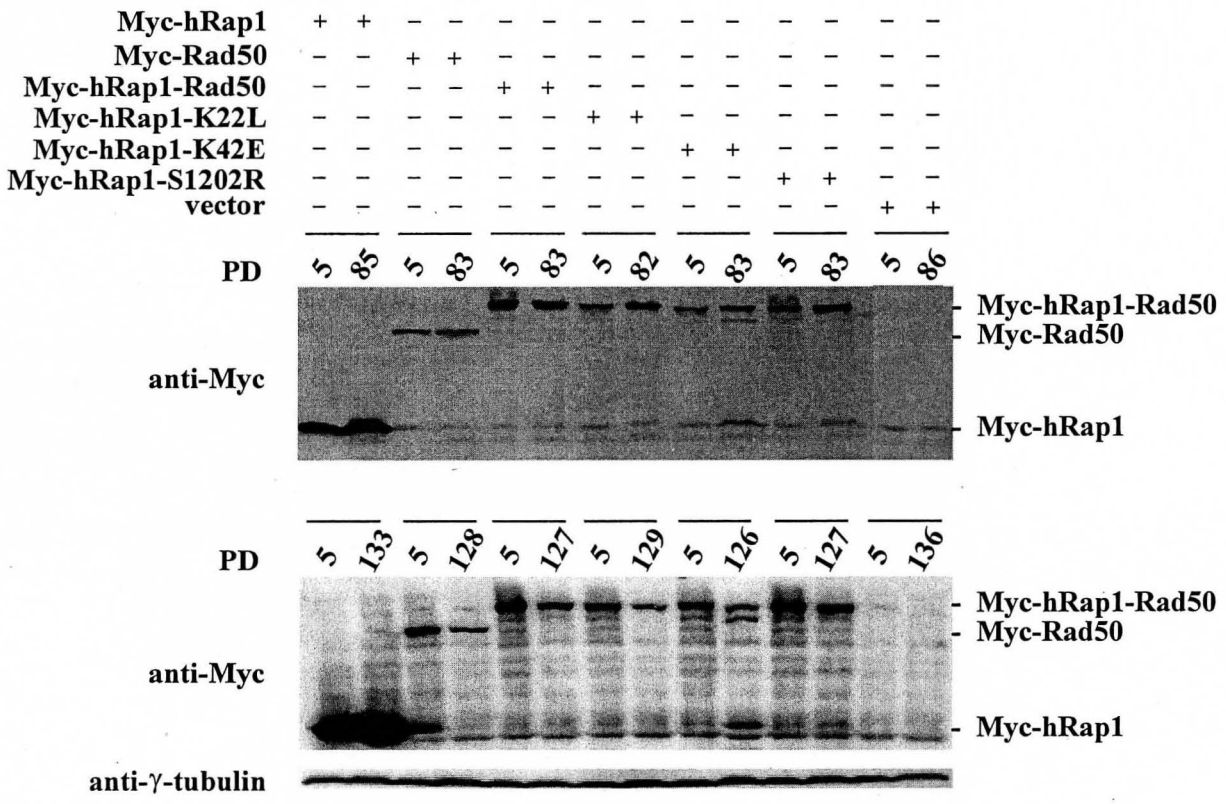
Myc-hRap1 + + − − − − − − − − − − − −
Myc-Rad50 − − + + − − − − − − − − − −
Myc-hRap1-Rad50 − − − − + + − − − − − − − −
Myc-hRap1-K22L − − − − − − + + − − − − − −
Myc-hRap1-K42E − − − − − − − − + + − − − −
Myc-hRap1-S1202R − − − − − − − − − − + + − −
vector − − − − − − − − − − − − + +
PD
5 85 5 83 5 83 5 82 5 83 5 83 5 86
anti-Myc
Myc-hRap1-Rad50
Myc-Rad50
Myc-hRap1
PD
5 133 5 128 5 127 5 129 5 126 5 127 5 136
anti-Myc
Myc-hRap1-Rad50
Myc-Rad50
Myc-hRap1
anti-γ-tubulin

Figure 3.9: Telomere length analysis in HT1080 cell lines expressing vector, hRap1, Rad50 and hRap1 fused Rad50 proteins. Genomic DNA was prepared from HT1080 cells grown for the indicated number of population doublings. The DNA was restricted with HinfI/RsaI and following southern blotting was hybridized with a probe specific for telomeric restriction fragments. The median telomere length of each cell line was plotted against population doublings. Wild-type hRap1-Rad50 caused telomere lengthening whereas the two defective mutants, hRap1-K42E and hRap1-S1202R did not. Vector control, hRap1 and Rad50 did not cause obvious telomere length change. (I would like to acknowledge Dr. Xu-Dong Zhu for her help in analyzing the data in this figure and for making this figure.)

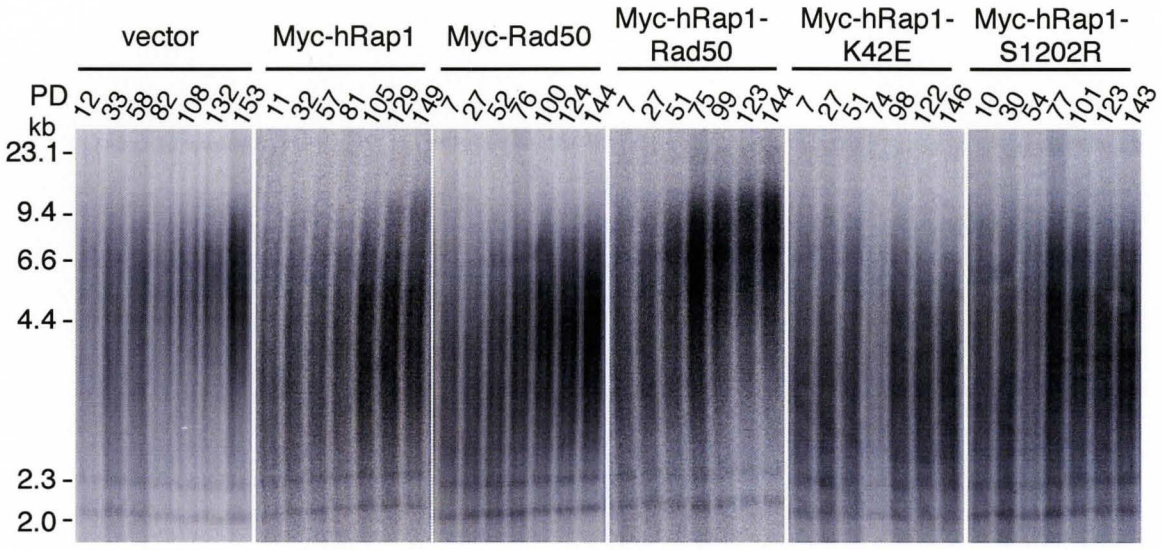
vector
Myc-hRap1
Myc-Rad50
Myc-hRap1-Rad50
Myc-hRap1-K42E
Myc-hRap1-S1202R
PD
12 33 58 82 108 132 153
11 32 57 81 105 129 149
7 27 52 76 100 124 144
7 27 51 75 99 123 144
7 27 51 74 98 122 146
10 30 54 77 101 123 143
kb
23.1
9.4
6.6
4.4
2.3
2.0

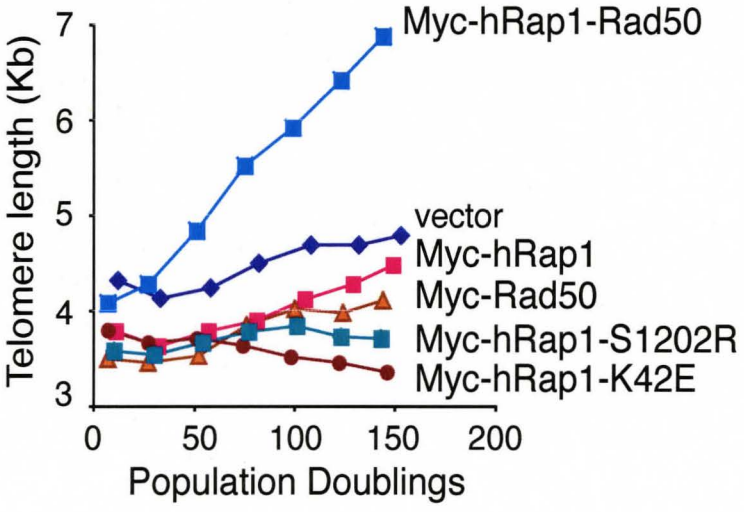
Telomere length (Kb)
7
6
5
4
3
0
50
100
150
200
Population Doublings
Myc-hRap1-Rad50
vector
Myc-hRap1
Myc-Rad50
Myc-hRap1-S1202R
Myc-hRap1-K42E

Figure 3.10: Expression of hRap1-fused Rad50 proteins in primary IMR90 cell lines. a) Western blotting showing expression level of Rad50 proteins in primary IMR90 cells. Cell extracts from primary IMR90 cells expressing various constructs were used for western analysis. The expression of Myc-hRap1 is much stronger than that of Rad50 proteins. Myc-Rad50, Myc-hRap1-Rad50 and Myc-hRap1-S1202R have similar protein expression levels whereas the expression of Myc-hRap1-K42E is weak. b) Immunofluorescence was conducted by using anti-Myc (9E10) antibody in primary IMR90 cells. Only a fraction of cells expressed fusion Rad50 proteins.

a)

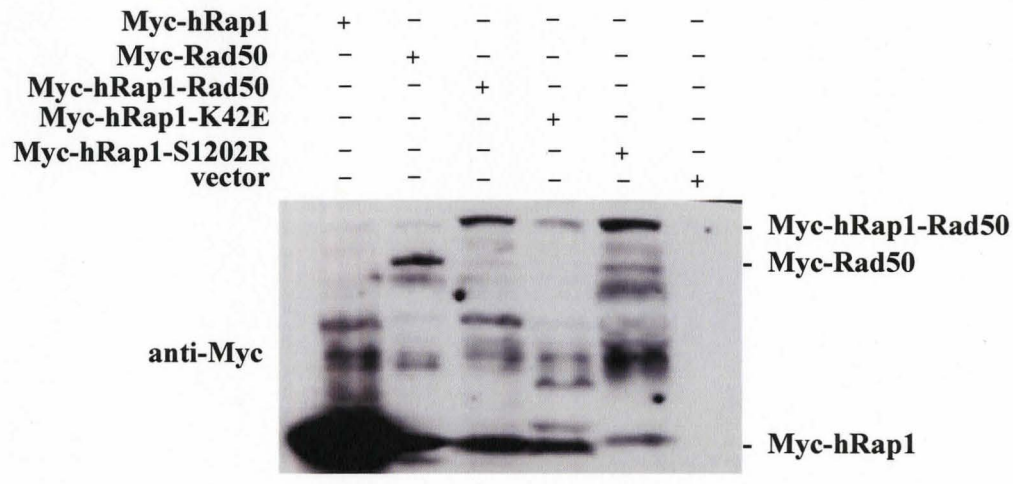
Myc-hRap1 + − − − − −
Myc-Rad50 − + − − − −
Myc-hRap1-Rad50 − − + − − −
Myc-hRap1-K42E − − − + − −
Myc-hRap1-S1202R − − − − + −
vector − − − − − +
anti-Myc
- Myc-hRap1-Rad50
- Myc-Rad50
- Myc-hRap1

b)

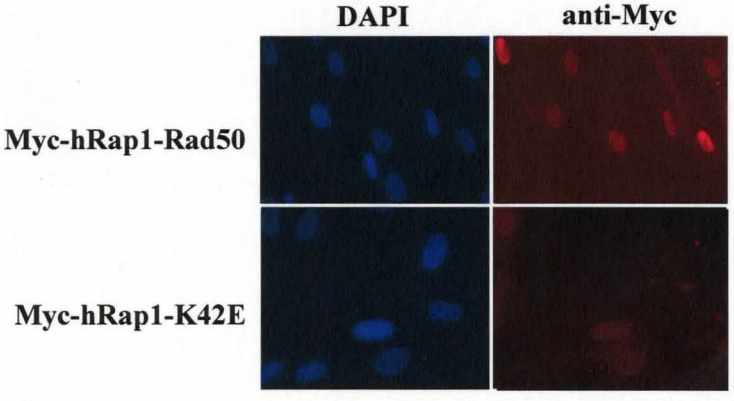
DAPI
anti-Myc
Myc-hRap1-Rad50
Myc-hRap1-K42E

Figure 3.11: hRap1-fused wild-type Rad50 but not mutant Rad50 is able to form irradiation-induced foci (IRIF). a) hRap1-fused wild-type Rad50 forms irradiation-induced foci in HT1080 cell lines but hRap1-K42E and hRap1-S1202R are defective in forming irradiation-induced foci. In addition, irradiation-induced foci of Rad50 co-localize with endogenous Mre11. Interphase HT1080 cells expressing various constructs were irradiated with 12 Gy and fixed 8 hours post irradiation. Immunofluorescence was conducted by using anti-Myc (9E10) (TRITC) and anti-Mre11 (FITC) primary antibody. b) Immunofluorescence showing irradiation-induced Myc-containing foci at 4 hours and 22 hours post irradiation in HT1080 cells expressing various constructs.

a)

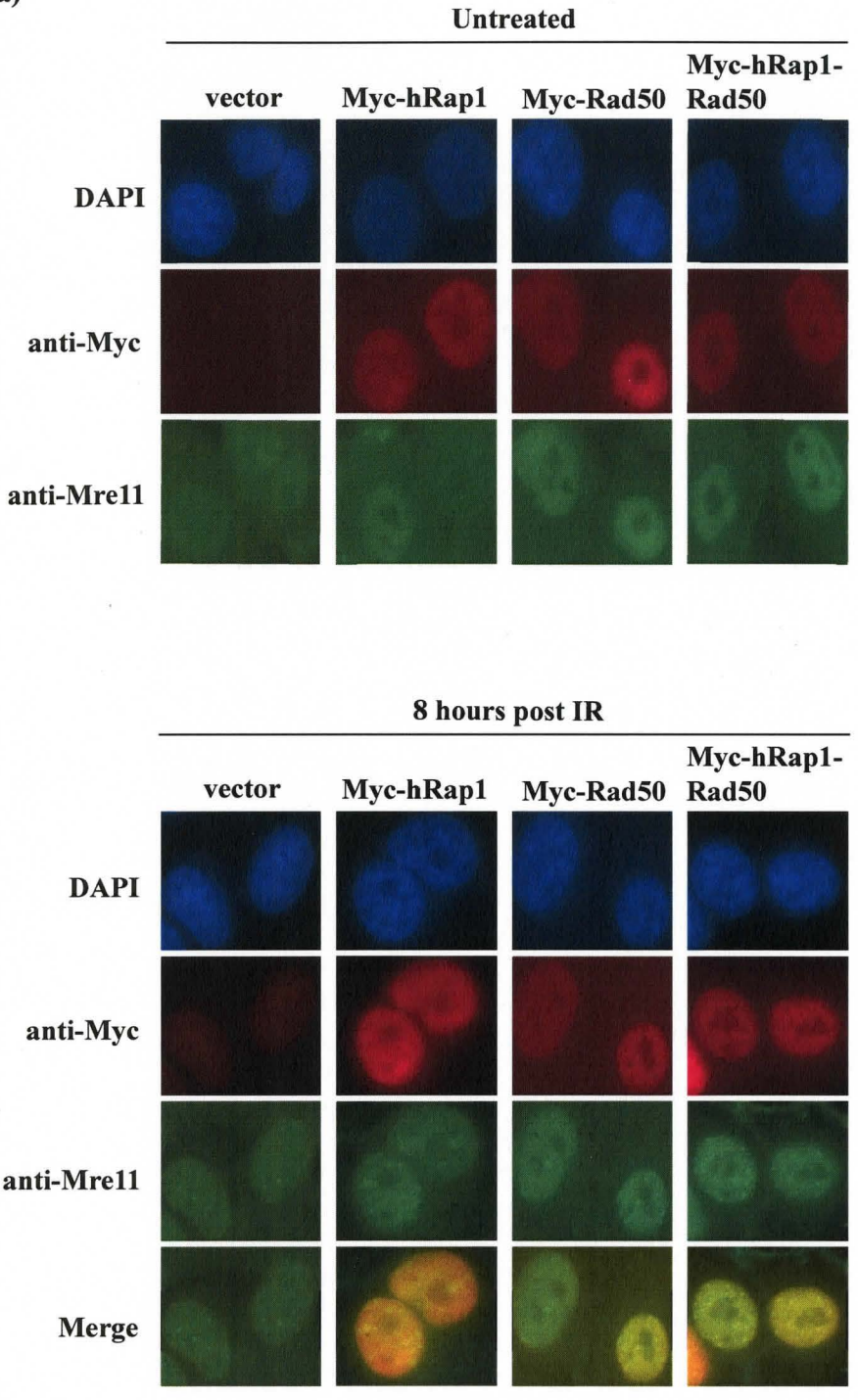
Untreated
vector
Myc-hRap1
Myc-Rad50
Myc-hRap1-Rad50
DAPI
anti-Myc
anti-Mre11
8 hours post IR
vector
Myc-hRap1
Myc-Rad50
Myc-hRap1-Rad50
DAPI
anti-Myc
anti-Mre11
Merge

b)

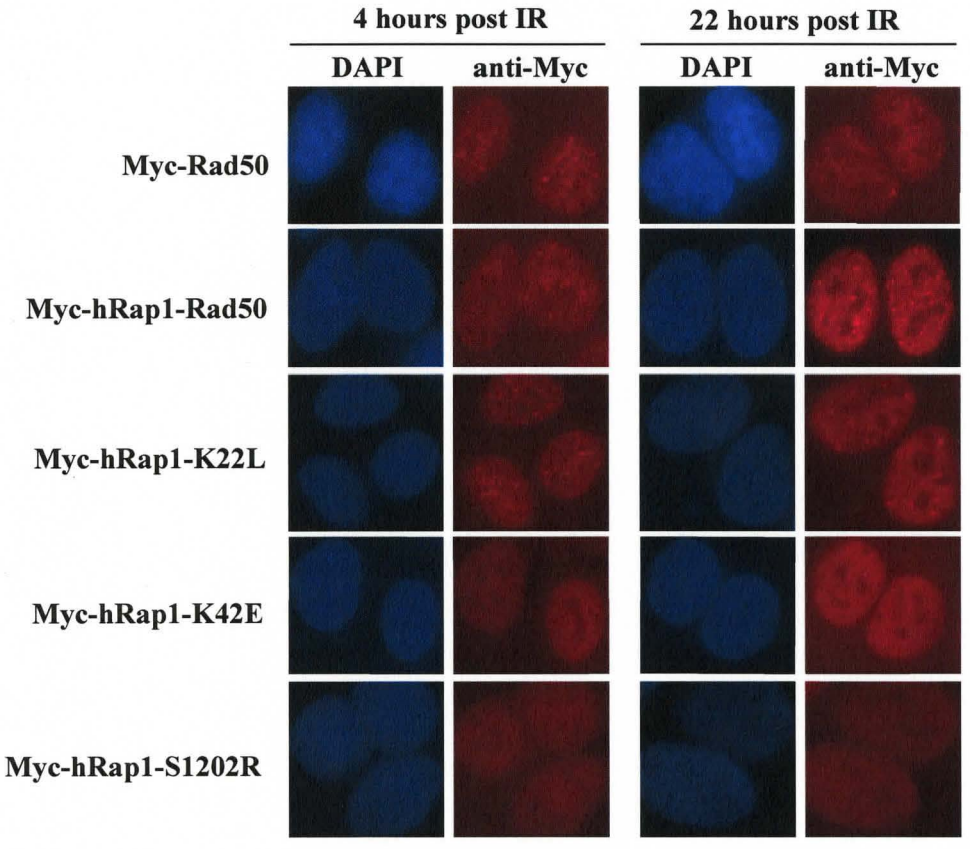
4 hours post IR
22 hours post IR
DAPI
anti-Myc
DAPI
anti-Myc
Myc-Rad50
Myc-hRap1-Rad50
Myc-hRap1-K22L
Myc-hRap1-K42E
Myc-hRap1-S1202R

Figure 3.12: The ability of endogenous Mre11 to form IRIF is defective in cells expressing hRap1-K42E and hRap1-S1202R. Interphase HT1080 cells expressing various constructs were irradiated with 12 Gy and fixed 8 hours post irradiation. Immunofluorescence was conducted with anti-Mre11 (FITC) antibody.

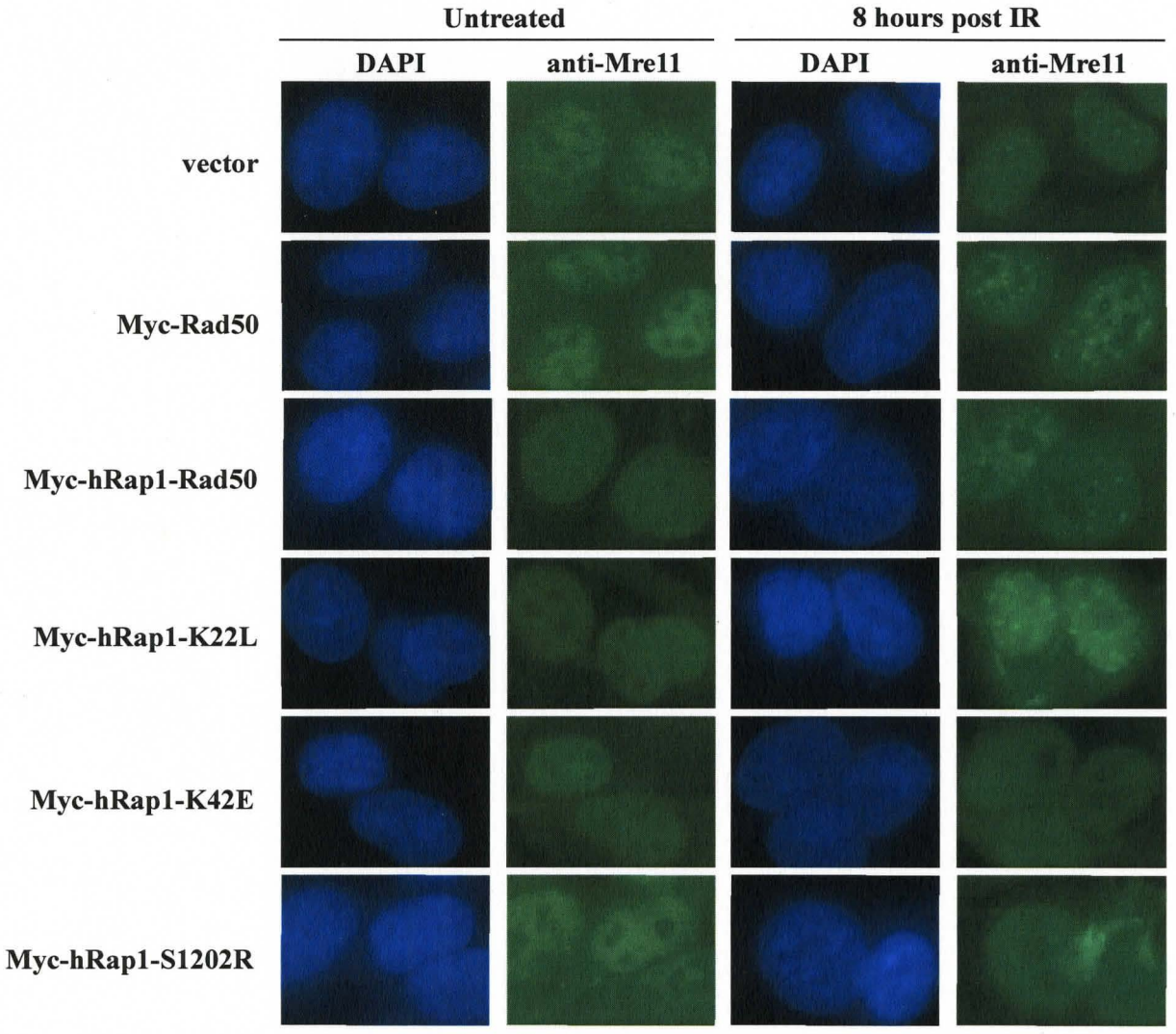
Untreated
8 hours post IR
DAPI
anti-Mre11
DAPI
anti-Mre11
vector
Myc-Rad50
Myc-hRap1-Rad50
Myc-hRap1-K22L
Myc-hRap1-K42E
Myc-hRap1-S1202R

Figure 3.13: Summary of irradiation-induced foci formation. Cells were irradiated at 12 Gy and fixed 4, 8 or 22 hours post irradiation. Nuclei containing five or more IRIF were counted as positive. Three independent experiments were conducted. More than five hundred cells were counted in each experiment. Standard deviations derived from three independent experiments are indicated. a) Percentage of nuclei having irradiation-induced Rad50 foci in HT1080 cells expressing various constructs 8 hours post irradiation. b) Percentage of nuclei having irradiation-induced Rad50 foci in HT1080 cells expressing various constructs 4 hours post irradiation. c) Percentage of nuclei having irradiation-induced Rad50 foci in HT1080 cells expressing various constructs 22 hours post irradiation. d) Percentage of nuclei having irradiation-induced endogenous Mre11 foci in HT1080 cells expressing various constructs 8 hours post irradiation.

a)

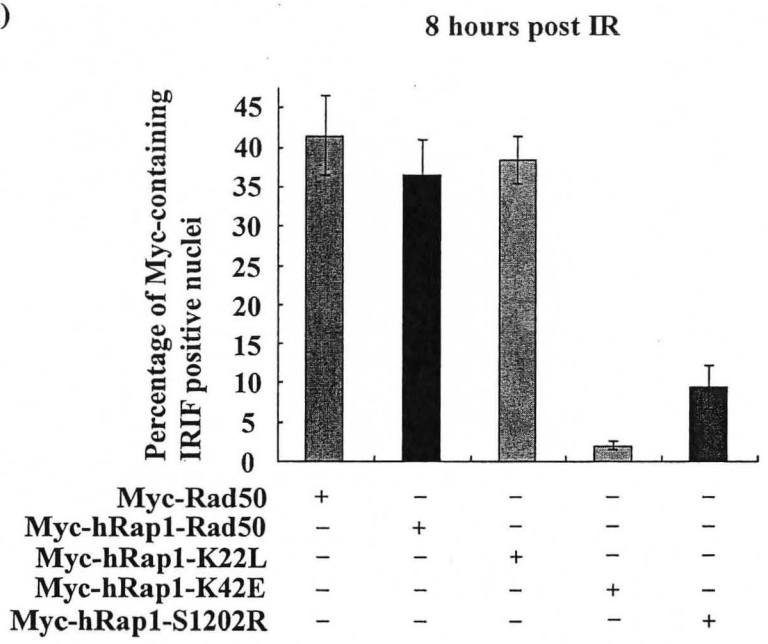
8 hours post IR
Percentage of Myc-containing IRIF positive nuclei
45
40
35
30
25
20
15
10
5
0
Myc-Rad50 + – – – –
Myc-hRap1-Rad50 – + – – –
Myc-hRap1-K22L – – + – –
Myc-hRap1-K42E – – – + –
Myc-hRap1-S1202R – – – – +

b)

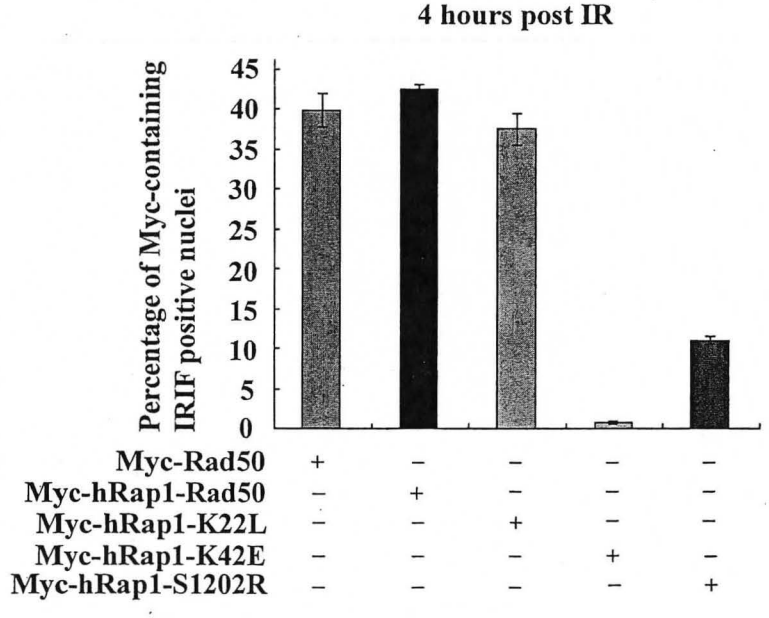
4 hours post IR
Percentage of Myc-containing IRIF positive nuclei
45
40
35
30
25
20
15
10
5
0
Myc-Rad50 + – – – –
Myc-hRap1-Rad50 – + – – –
Myc-hRap1-K22L – – + – –
Myc-hRap1-K42E – – – + –
Myc-hRap1-S1202R – – – – +

c)

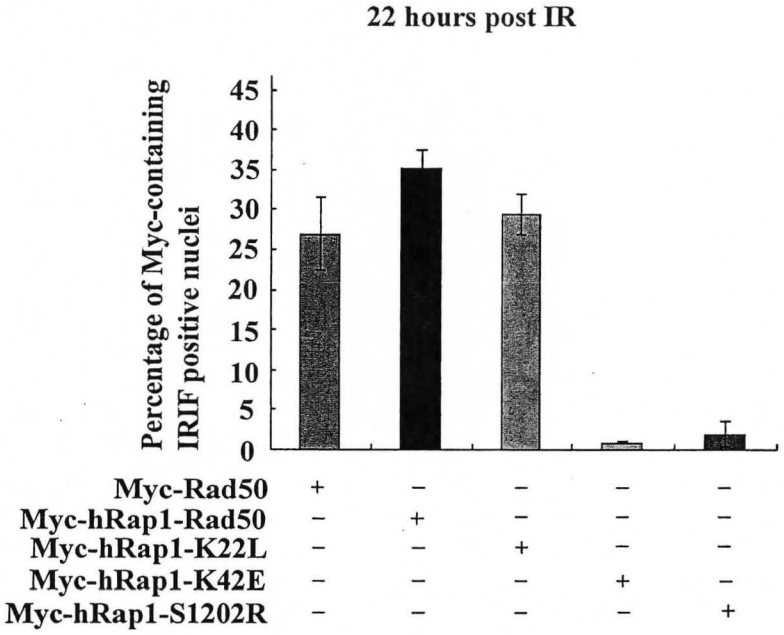
22 hours post IR
Percentage of Myc-containing IRIF positive nuclei
45
40
35
30
25
20
15
10
5
0
Myc-Rad50 + – – – –
Myc-hRap1-Rad50 – + – – –
Myc-hRap1-K22L – – + – –
Myc-hRap1-K42E – – – + –
Myc-hRap1-S1202R – – – – +

d)

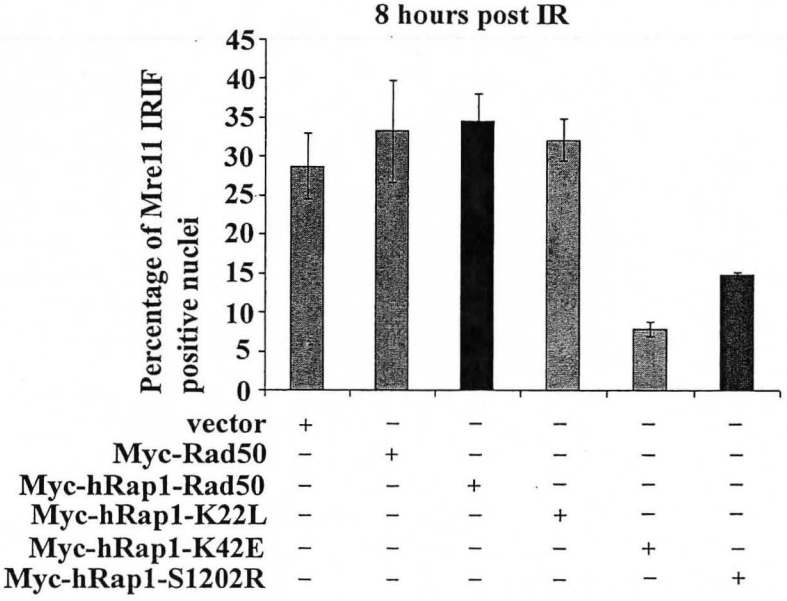
8 hours post IR
Percentage of Mre11 IRIF positive nuclei
45
40
35
30
25
20
15
10
5
0
vector + – – – – –
Myc-Rad50 – + – – – –
Myc-hRap1-Rad50 – – + – – –
Myc-hRap1-K22L – – – + – –
Myc-hRap1-K42E – – – – + –
Myc-hRap1-S1202R – – – – – +

Figure 3.14: Expression of dominant negative TRF2 allele ($TRF2^{\Delta B\Delta M}$) in HT1080 cell lines expressing Rad50 alleles. pWZL and pWZL-$TRF2^{\Delta B\Delta M}$ were introduced into HT1080 cell lines expressing vector, Myc-hRap1, Myc-Rad50 and fusion proteins by retrovirus infection. Cell extracts were collected and western blotting was conducted by using anti-TRF2 antibody. The expression levels of $TRF2^{\Delta B\Delta M}$ in HT1080 cell lines expressing vector, Myc-hRap1, Myc-Rad50 and fusion proteins are similar.

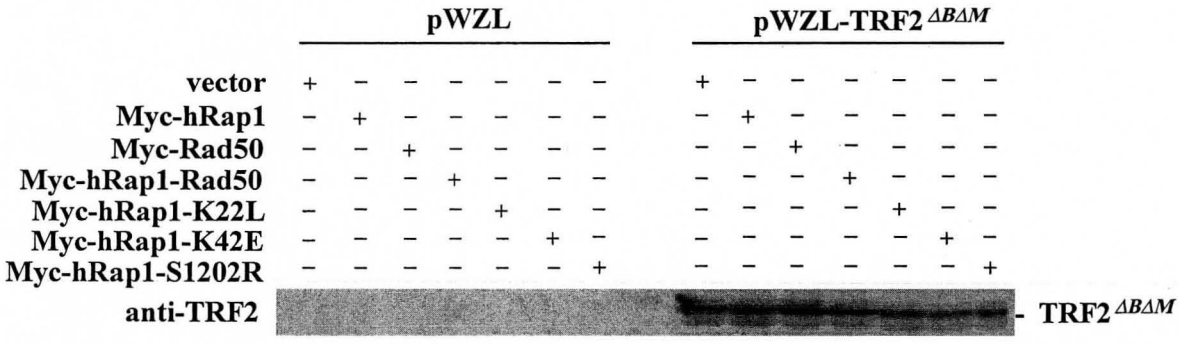
pWZL
pWZL-TRF2 ΔBΔM
vector + − − − − − − + − − − − − −
Myc-hRap1 − + − − − − − − + − − − − −
Myc-Rad50 − − + − − − − − − + − − − −
Myc-hRap1-Rad50 − − − + − − − − − − + − − −
Myc-hRap1-K22L − − − − + − − − − − − + − −
Myc-hRap1-K42E − − − − − + − − − − − − + −
Myc-hRap1-S1202R − − − − − − + − − − − − − +
anti-TRF2
- TRF2 ΔBΔM

Figure 3.15: Expression of the dominant negative TRF2 allele negatively regulate population growth of cells. pWZL and pWZL-TRF2$^{\Delta B\Delta M}$ was introduced into HT1080 cell lines expressing vector, Myc-hRap1, Myc-Rad50 and fusion proteins by retrovirus infection. 250 cells were plated each well on 24-well plates in triplicate at the fourth day of selection. Cell numbers in each well were counted every day in the following 19 days. Cells were split and re-plated when they got confluent. Relative cell number = Cell number in the well × split ratio. Relative cell number of cell lines with or without TRF2$^{\Delta B\Delta M}$ was plotted against time. Both regular scale and log scale of average numbers ± standard deviation from triplicate wells are shown. Similar trends were observed in two independent infections. Expressing defective Rad50 mutants did not affect sensing of uncapped telomeres. a) Growth curve of cells expressing vector/pWZL and vector/pWZL-TRF2$^{\Delta B\Delta M}$. b) Log scale of Fig a. c) Growth curve of cells expressing Myc-hRap1/pWZL and Myc-hRap1/pWZL-TRF2$^{\Delta B\Delta M}$. d) Log scale of Fig c. e) Growth curve of cells expressing Myc-Rad50/pWZL and Myc-Rad50/pWZL-TRF2$^{\Delta B\Delta M}$. f) Log scale of Fig e. g) Growth curve of cells expressing Myc-hRap1-Rad50/pWZL and Myc-hRap1-Rad50/pWZL-TRF2$^{\Delta B\Delta M}$. h) Log scale of Fig g. i) Growth curve of cells expressing Myc-hRap1-Rad50 K22L/pWZL and Myc-hRap1-Rad50 K22L/pWZL-TRF2$^{\Delta B\Delta M}$. j) Log scale of Fig i. k) Growth curve of cells expressing Myc-hRap1-Rad50 K42E/pWZL and Myc-hRap1-Rad50 K42E/pWZL-TRF2$^{\Delta B\Delta M}$. l) Log scale of Fig k. m) Growth curve of cells expressing Myc-hRap1-Rad50 S1202R/pWZL and Myc-hRap1-Rad50 S1202R/pWZL-TRF2$^{\Delta B\Delta M}$. n) Log scale of Fig m.

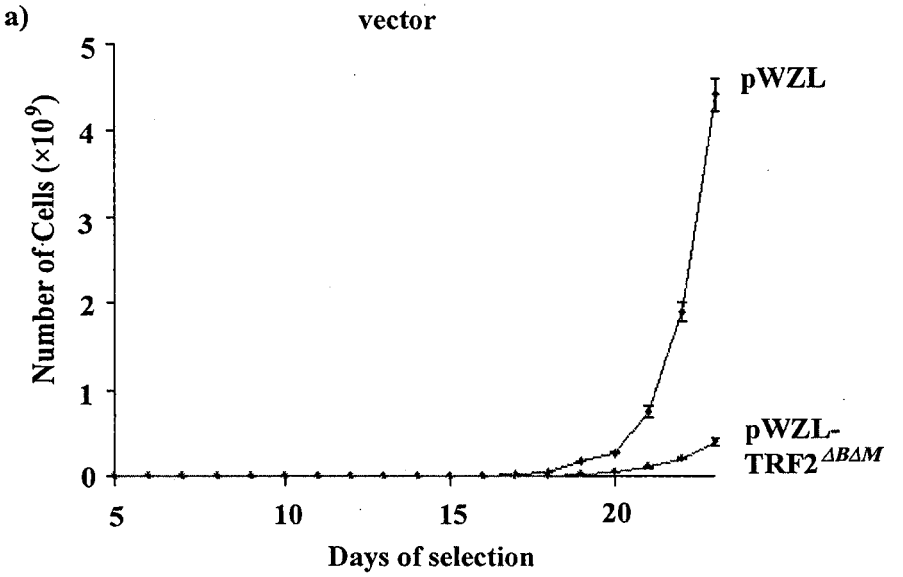
a)
vector
Number of Cells (×10^9)
5
4
3
2
1
0
5
10
15
20
Days of selection
pWZL
pWZL-
TRF2 ΔBΔM

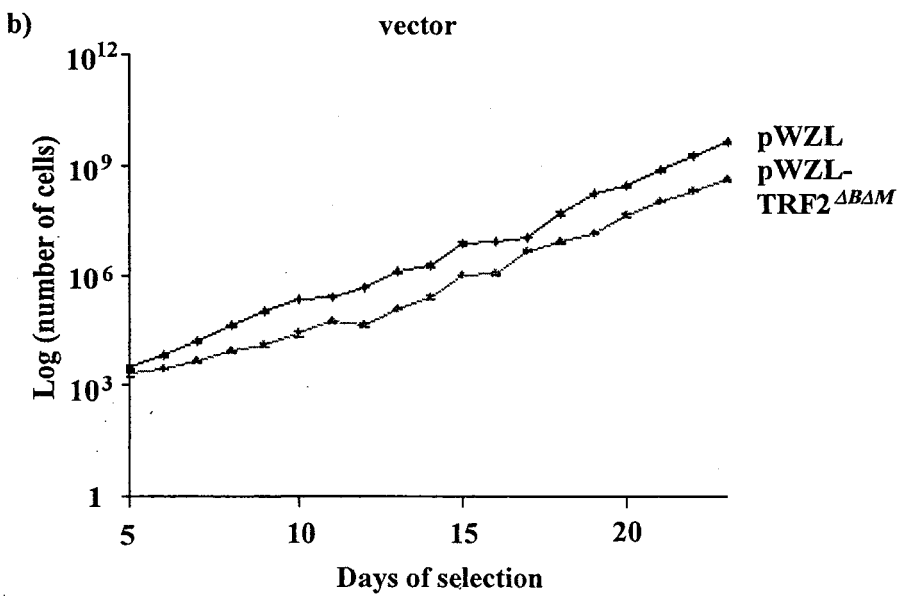
b)
vector
Log (number of cells)
10^12
10^9
10^6
10^3
1
5
10
15
20
Days of selection
pWZL
pWZL-
TRF2 ΔBΔM

c)

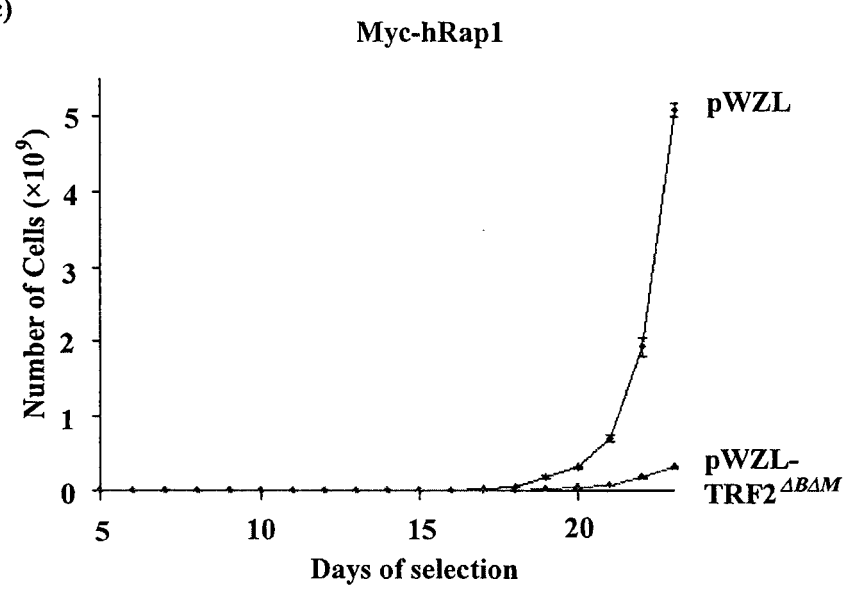
Myc-hRap1
Number of Cells (×10^9)
0
1
2
3
4
5
5
10
15
20
Days of selection
pWZL
pWZL-
TRF2 ΔBΔM

d)

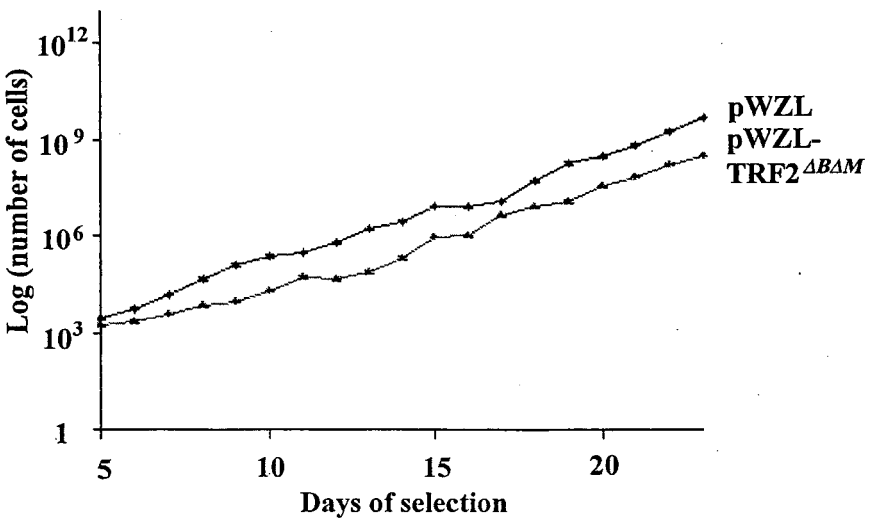
Myc-hRap1
Log (number of cells)
10^12
10^9
10^6
10^3
1
5
10
15
20
Days of selection
pWZL
pWZL-
TRF2 ΔBΔM

e)

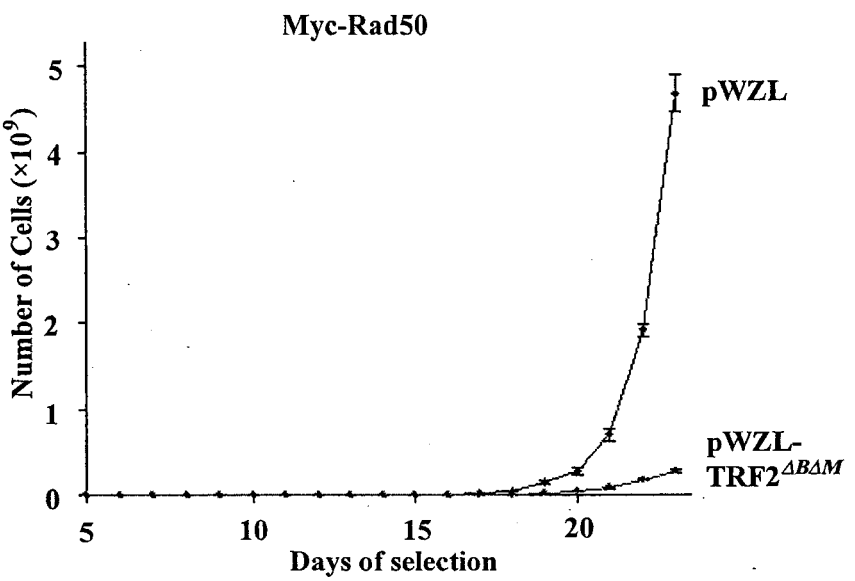
Myc-Rad50
Number of Cells (×10^9)
5
4
3
2
1
0
5
10
15
20
Days of selection
pWZL
pWZL-
TRF2^ΔBΔM

f)

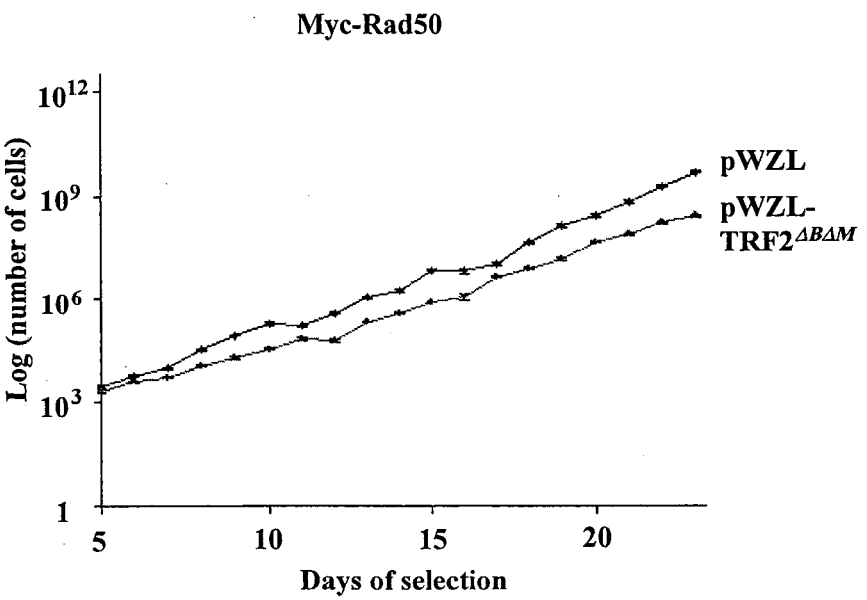
Myc-Rad50
Log (number of cells)
10^12
10^9
10^6
10^3
1
5
10
15
20
Days of selection
pWZL
pWZL-
TRF2^ΔBΔM

g)

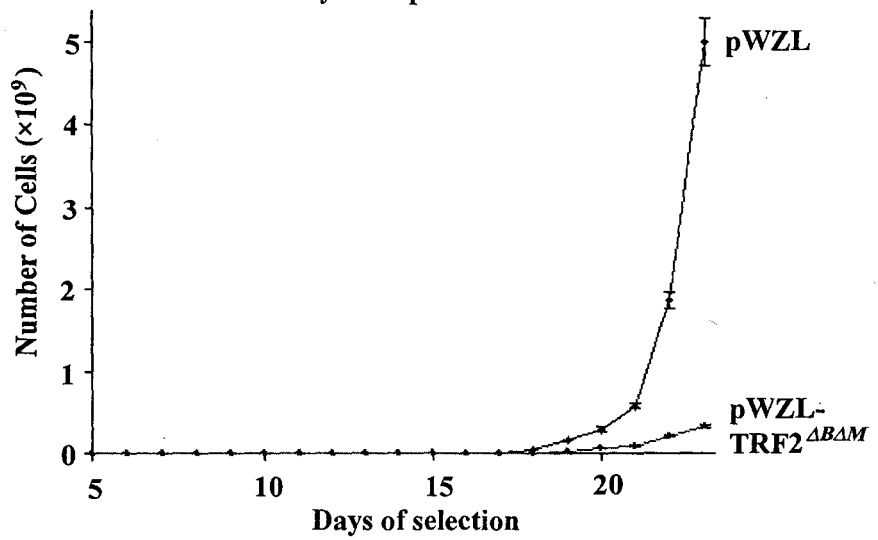
Myc-hRap1-Rad50
Number of Cells (×10⁹)
5
4
3
2
1
0
5
10
15
20
Days of selection
pWZL
pWZL-
TRF2 ΔBΔM

h)

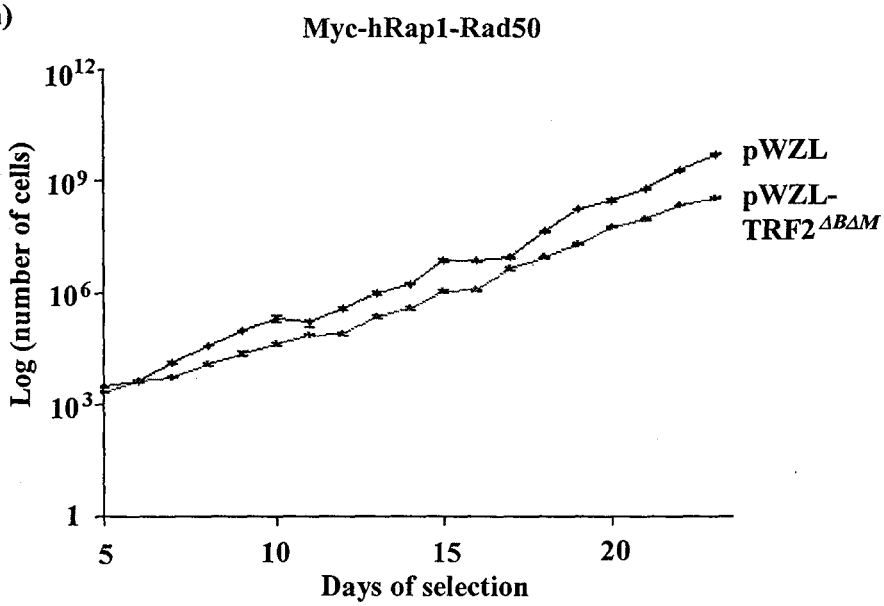
Myc-hRap1-Rad50
Log (number of cells)
10¹²
10⁹
10⁶
10³
1
5
10
15
20
Days of selection
pWZL
pWZL-
TRF2 ΔBΔM

i)

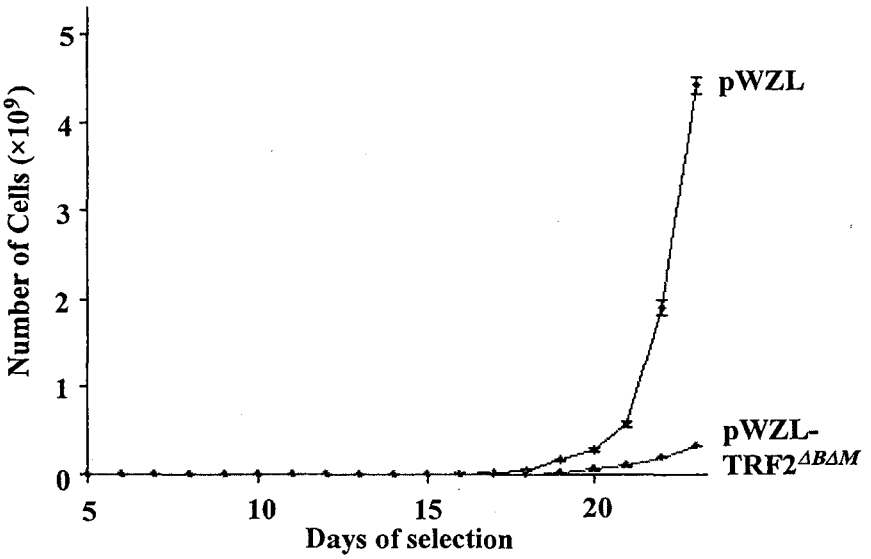
Myc-hRap1-K22L
Number of Cells (×10^9)
5
4
3
2
1
0
5
10
15
20
Days of selection
pWZL
pWZL-
TRF2^ΔBΔM

j)

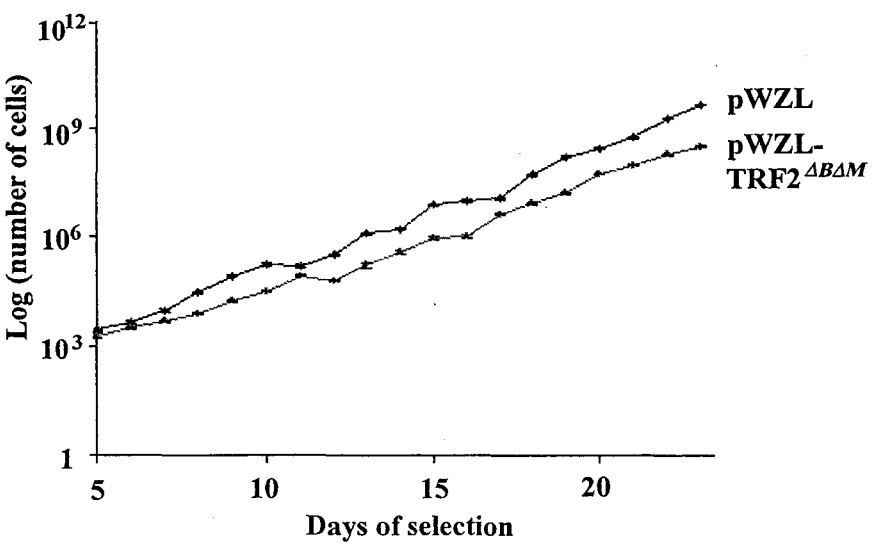
Myc-hRap1-K22L
Log (number of cells)
10^12
10^9
10^6
10^3
1
5
10
15
20
Days of selection
pWZL
pWZL-
TRF2^ΔBΔM

k)

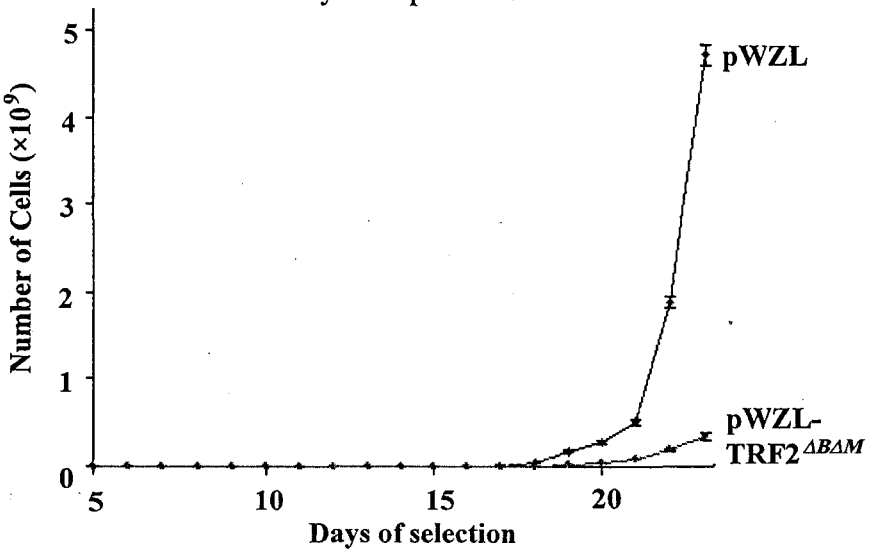
Myc-hRap1-K42E
Number of Cells (×10^9)
5
4
3
2
1
0
5
10
15
20
Days of selection
pWZL
pWZL-
TRF2^ΔBΔM

l)

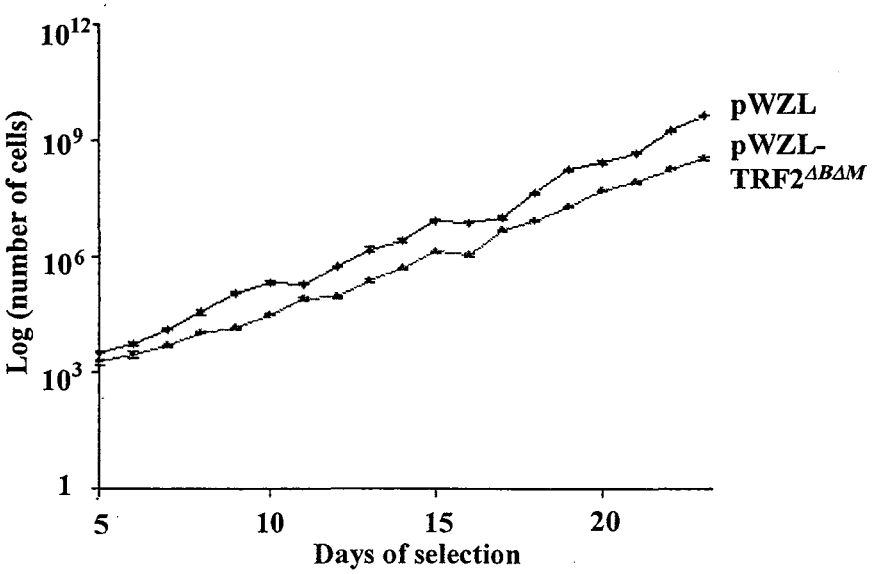
Myc-hRap1-K42E
Log (number of cells)
10^12
10^9
10^6
10^3
1
5
10
15
20
Days of selection
pWZL
pWZL-
TRF2^ΔBΔM

m)

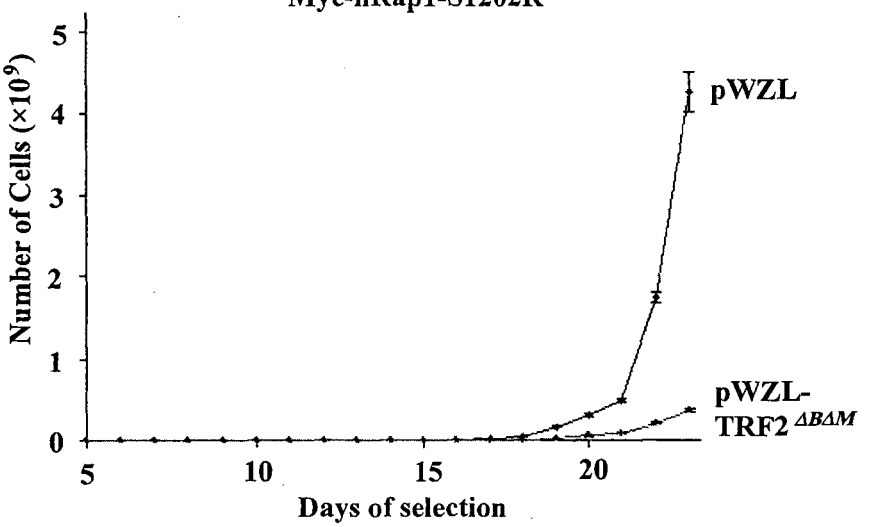
Myc-hRap1-S1202R
Number of Cells (×10^9)
5
4
3
2
1
0
5
10
15
20
Days of selection
pWZL
pWZL-
TRF2 ΔBΔM

n)

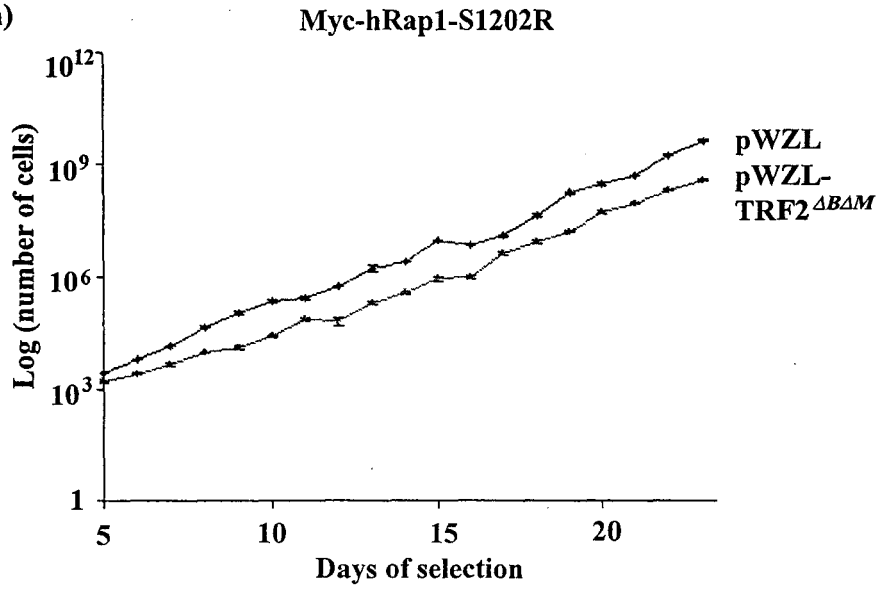
Myc-hRap1-S1202R
Log (number of cells)
10^12
10^9
10^6
10^3
1
5
10
15
20
Days of selection
pWZL
pWZL-
TRF2 ΔBΔM

Figure 3.16: Phosphorylation of γ-H2AX in HT1080 cell lines in response to irradiation. Whole cell extracts from HT1080 cells expressing various constructs were made at different time points post 12 Gy irradiation. Western blotting was conducted with anti-phosphorylated γ-H2AX (Ser139) antibody. Dynamics of phosphorylated γ-H2AX were similar in cell lines expressing vector, Myc-hRap1-Rad50, Myc-hRap1-Rad50 K42E and Myc-hRap1-Rad50 S1202R. Anti-H2AX blot was used as a loading control.

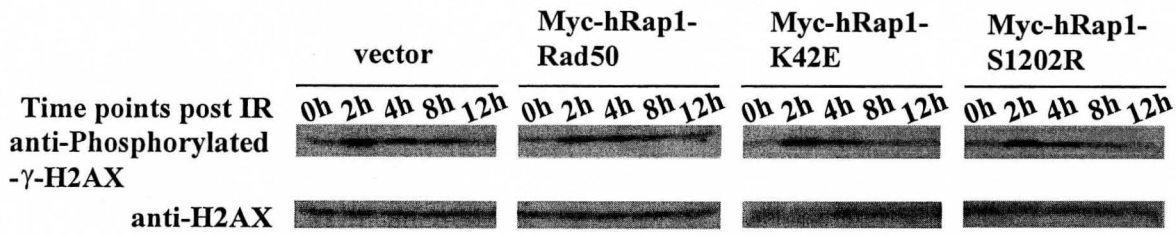
vector
Myc-hRap1-Rad50
Myc-hRap1-K42E
Myc-hRap1-S1202R
Time points post IR
0h 2h 4h 8h 12h
0h 2h 4h 8h 12h
0h 2h 4h 8h 12h
0h 2h 4h 8h 12h
anti-Phosphorylated -γ-H2AX
anti-H2AX

Chapter 4

Discussion

4.1 Rad50 is a positive regulator of telomere length

In order to examine the role of Rad50 on telomere length regulation, two defective mutants of Rad50 were constructed in the study. The mutants K42E and S1202R contain mutations in Walker A and Signature motif respectively. Both mutants were shown defective in ATP-dependent activities *in vitro* (Paull and Gellert 1999; Lee and Paull 2004; Lee and Paull 2005). However, overexpression of these two mutants in HT1080 cell line was predominantly in cytoplasm, making it difficult to investigate their impact on telomeres. Therefore, a fusion strategy was used to target the proteins to nucleus, especially onto telomeres. The immunofluorescence data indicated that fusing to hRap1 not only targets these mutants into nucleus, but also specifically increases the expressed proteins at telomeres (Figure 3.5). The co-immunoprecipitation data also revealed that fusion proteins were successfully brought to TRF2 complex on telomeres. In addition, compared to unfused Rad50, fusion proteins brought down more TRF2 (Figure 3.6). Since the amounts and properties of unfused Rad50

and endogenous Rad50 were similar, it is likely that fusion Rad50 proteins have higher ability of binding to TRF2 compared to endogenous Rad50. In addition, my colleague Yili Wu did chromatin immunoprecipitation which also showed that fusion of hRap1 results in an increase in the amount of Rad50 proteins at telomeres. These results suggest that the fusion approach made it possible to study the function of Rad50 at telomeres since it create a local overexpression environment at telomeres.

A series of experiments were conducted to examine whether the property of Rad50 was still preserved in the context of the fusion protein. The results presented here showed that fusion proteins were able to interact with its partner Mre11 at a level comparable to that of unfused Rad50. In addition, the ability of wild-type Rad50 to form irradiation-induced foci was not affected by fusing to hRap1. These results suggest that fusing Rad50 to hRap1 did not damage the function of Rad50 protein.

I have shown that Myc-hRap1-Rad50 induced telomere lengthening, which is telomerase dependent in HT1080 cell line. This phenotype was not seen in Myc-hRap1 expressing cell line, which indicated that telomere lengthening is not caused by the hRap1 portion of the fusion protein. The Rad50 expressing cell line also did not have telomere lengthening because of the limited amount of Rad50 protein on telomeres. By fusing to hRap1, the amount of Rad50 protein on telomeres increased and telomeres got lengthened subsequently. Given those facts, we reasoned that Rad50 might be a positive regulator of telomere length.

The Myc-hRap1-Rad50 K22L mutant showed a similar telomere lengthening with Myc-hRap1-Rad50 in the first 100 PD (data not shown), which is consistent with our hypothesis that it is similar to K22M which is a "gain-of-function" mutation (Bender *et al.* 2002; Morales *et al.* 2005). The two defective mutants did not cause telomere lengthening

up to about 150 PD. The protein expression levels of Myc-hRap1-Rad50, Myc-hRap1-Rad50 K42E and Myc-hRap1-Rad50 S1202R did not have dramatic fluctuation during cell culture and the location of fusion proteins has been demonstrated by immunofluorescence. This indicated that those phenotypes can truly reflect the function of Rad50 proteins on telomeres. The fact that fusion wild-type Rad50 rather than the two defective mutants caused telomere lengthening suggested that the ATP related activities of Rad50 contribute to telomerase dependent telomere maintenance in human cell lines.

To further confirm that the telomere phenotype is through a telomerase dependent pathway, all the Rad50 alleles were introduced into normal human fibroblast that are telomerase negative. The alleles were introduced into IMR90 cell line by Yili Wu. As shown in Figure 3.10, Western blot and IF were conducted to examine the expression level of the expressed proteins. However, from IF using anti-Myc antibodies, only part of the cells expressed the fusion proteins (about 40% in Myc-hRap1-Rad50 cell line). In the Myc-hRap1-Rad50 K42E expressing cell line, the percentage was even lower (about 10%). Furthermore, this cell line started entering senescence after one month cell culture. Consequently, it is difficult to examine telomere length change or DSB repair processes after irradiation in those cell lines.

Expressing Rad50 alleles was attempted in WI38VA13/2RA cell line, which is also telomerase negative. This cell line is dependent on ALT (alternative telomere lengthening) pathway to maintain telomeres (Wu *et al.* 2000; Jiang *et al.* 2005). However, only about 30% of the cells had expression (data not shown), which makes it difficult to conduct further study.

The fact that hRap1 fused Rad50 caused telomere lengthening suggests that MRN has a positive role in telomere maintenance. Future work could be carried out to uncover

the mechanism underlying this phenotype.

4.2 Rad50 mutants defective in ATP-dependent activities fail to accumulate on DSB sites

The second line of the study lied in another finding: the two defective mutants were not able to form obvious irradiation-induced foci. It suggested that the mutations within catalytic Walker A domain and Signature motif affect the ability of Rad50 protein of forming irradiation-induced foci (IRIF). In addition, expressing two defective mutants also affected endogenous Mre11 forming IRIF. We reasoned that they might be functioning in a dominant negative way. Although the functions corresponding to the formation of MRN IRIF in DNA double-strand repair were not known yet, we also did several experiments in order to uncover which step in this process might be affected by expressing these two defective mutants.

It has been well established that introducing a dominant negative allele of TRF2 ($TRF2^{\Delta B\Delta M}$) into cells can induce dysfunctional telomeres, which triggered cellular response similar to DNA double-strand break (van Steensel *et al.* 1998; de Lange 2002; Jacobs and de Lange 2005). Van Steensel reported that growth arrest was observed after introducing $TRF2^{\Delta B\Delta M}$ into HTC75 cell line, which is a colonial cell line derived from HT1080 cell line. To examine whether the Rad50 mutants affect sensing dysfunctional telomere, vector (pWZL) and $TRF2^{\Delta B\Delta M}$ were introduced into HT1080 cell lines containing different Rad50 alleles. The results show slower population growth rather than growth arrest in dominant negative TRF2 allele expressing cell lines, compared with vector control. This might be due to the slight different features of these cell lines or the retrovirus

infection method we used could not induce robust TRF2$^{\Delta B\Delta M}$ expression into every single cell.

Strikingly, the Myc-hRap1- Rad50 K42E/TRF2$^{\Delta B\Delta M}$ and Myc-hRap1- Rad50 S-1202R/ TRF2$^{\Delta B\Delta M}$ expressing cell lines also showed slower population doubling rate as the control cell lines did. Thus expressing these two defective mutants did not induce detectable difference in sensing uncapped telomeres. It might be possible that the fusion protein lost the advantage of binding to telomeres in absence of TRF2 on telomeres compared to endogenous Rad50 protein or the endogenous protein was enough to induce slower population growth in a relatively long time period. Another possibility might be that the difference of population growth rate is too subtle to detect in tumor cell lines.

It has been established that telomere fusions caused by introducing TRF2$^{\Delta B\Delta M}$ are dependent on NHEJ pathway whereas telomere deletions caused by introducing TRF2$^{\Delta B}$ are dependent on HR pathway (Smogorzewska and de Lange 2002; Wang *et al.* 2004). I attempted to examine the Rad50's role in these repair pathways. Efforts were conducted to count the frequency of anaphase bridges in HT1080 cell lines expressing both TRF2$^{\Delta B\Delta M}$ and hRap1 fused Rad50 alleles. However, since the background of chromosome abnormality is too high in cancer cell line, we were not been able to get conclusive data. I also attempted to compare the TRF2$^{\Delta B}$ induced telomere loss in cells expressing different Rad50 alleles by southern blotting. Unfortunately, we failed to accurately quantify the telomere loss.

In the context of dysfunctional telomeres, TRF2$^{\Delta B\Delta M}$ experiments could be repeated in normal cell lines in order to count anaphase bridges at a cleaner background. Other techniques, such as 2D gel which can detect the deleted circular DNA from telomeres, could be used to analysis the telomere loss caused by introducing TRF2$^{\Delta B}$.

Besides the experiments of dysfunctional telomeres, I also did several experiments to investigate the role of Rad50 in DNA double-strand break repair. In order to examine the repair efficiency of DSB, I observed the kinetics of phosphorylation of γ-H2AX at Serine139 by western blotting. No significant difference of presence or decrease of γ-H2AX phosphorylation was detected among cell lines expressing Rad50 alleles. γ-H2AX is phosphorylated at Serine139 by PIKK family members (ATM, ATR and DNA-PKcs) shortly post irradiation and the decrease of phosphorylated form of γ-H2AX reflects the repair process of DSBs. It suggested that the repair process in HT1080 cell line was not affected by expressing Rad50 mutants.

In addition, I have observed ATM phosphorylation by IF shortly after IR treatment in fused Rad50 mutants expressing cell lines, similar with that in fused wild-type Rad50 expressing cells (data not shown). Maybe expressing defective Rad50 mutants is not sufficient enough to block ATM activation in the presence of endogenous Rad50 protein in nucleoplasm. Due to the difficulty of expressing these fusion Rad50 alleles in normal cells, we were not able to examine the phosphorylation of substrates of ATM, such as p53.

4.3 Future work to examine the role of MRN in DNA damage repair

In our work, we did not observe blocking of sensing DNA double-strand break or dysfunctional telomeres in HT1080 cell lines expressing Rad50 mutants. There are two possible explanations: first, the effects of expressing mutants might be attenuated by the endogenous Rad50 proteins. Second, the cell line used in the study lacks intact checkpoints. This made it difficult to further examine the role of MRN in sensing DNA damage. To gain

more understanding on the role of MRN in sensing DNA damage, future studies should be focused on improving the expression of Rad50 proteins and expressing Rad50 alleles in normal cell lines. A nuclear localization sequence could be used to introduce Rad50 alleles into normal cells. Then experiments can be carried out to examine the activation of cell cycle checkpoint proteins responding to DNA damage.

The results revealed that dynamics of phosphorylation of γ-H2AX did not change in cells expressing Rad50 mutants comparing to wild-type Rad50. This suggests that the repair process is not affected in cells expressing Rad50 mutants. However, since there are two pathways of DSB repair in human cells (HR and NHEJ) (Su 2006), we can not rule out the possibility that the Rad50 mutants may affect one of the repair pathway but not the other. Future study can be carried out to examine this by blocking one of the two pathways. To do this, PIKK inhibitors or deficient cell lines could be used to examine the role of MRN in the other pathway.

Bibliography

Assenmacher, N. and K. P. Hopfner (2004). MRE11/RAD50/NBS1: complex activities. *Chromosoma 113*, 157–166.

Bai, Y. and J. P. Murnane (2003). Telomere instability in a human tumor cell line expressing NBS1 with mutations at sites phosphorylated by ATM. *Mol Cancer Res 1*, 1058–1069.

Baumann, P. and S. C. West (1998). Role of the human RAD51 protein in homologous recombination and double-stranded break repair. *Trends Biochem Sci 23*, 247–251.

Bender, C. F., M. L. Sikes, R. Sullivan, L. E. Huye, M. M. Le Beau, D. B. Roth, O. K. Mirzoeva, E. M. Oltz, and J. H. Petrini (2002). Cancer predisposition and hematopoietic failure in Rad50(S/S) mice. *Genes Dev 16*, 2237–2251.

Bianchi, A., S. Smith, L. Chong, P. Elias, and T. de Lange (1997). TRF1 is a dimer and bends telomeric DNA. *EMBO J 16*, 1785–1794.

Bianchi, A., R. M. Stansel, L. Fairall, J. D. Griffith, D. Rhodes, and T. de Lange (1999). TRF1 binds a bipartite telomeric site with extreme spatial flexibility. *EMBO J 18*, 5735–5744.

Boulton, S. J. and S. P. Jackson (1998). Components of the ku-dependent non-homologous end-joining pathway are involved in telomeric length maintenance and

telomeric silencing. *EMBO J 17*, 1819–1828.

Bressan, D. A., B. K. Baxter, and J. H. Petrini (1999). The Mre11-Rad50-Xrs2 protein complex facilitates homologous recombination-based double-strand break repair in *Saccharomyces cerevisiae*. *Mol Cell Biol 19*, 7681–7687.

Buscemi, G., C. Savio, L. Zannini, F. Micciche, D. Masnada, M. Nakanishi, H. Tauchi, K. Komatsu, S. Mizutani, K. Khanna, P. Chen, P. Concannon, L. Chessa, and D. Delia (2001). Chk2 activation dependence on Nbs1 after DNA damage. *Mol Cell Biol 15*, 5214–5222.

Carson, C. T., R. A. Schwartz, T. H. Stracker, C. E. Lilley, D. V. Lee, and M. D. Weitzman (2003). The Mre11 complex is required for ATM activation and the G2/M checkpoint. *EMBO J 22*, 6610–6620.

Chai, W., A. J. Sfeir, H. Hoshiyama, J. W. Shay, and W. E. Wright (2006). The involvement of the Mre11/Rad50/Nbs1 complex in the generation of G-overhangs at human telomeres. *EMBO Rep 7*, 225–230.

Chen, L., K. M. Trujillo, S. Van Komen, D. H. Roh, L. Krejci, L. K. Lewis, M. A. Resnick, P. Sung, and A. E. Tomkinson (2005). Effect of amino acid substitutions in the rad50 ATP binding domain on DNA double strand break repair in yeast. *J Biol Chem. 280*, 2620–2627.

Chong, L., B. van Steensel, D. Broccoli, H. Erdjument-Bromage, J. Hanish, P. Tempst, and T. de Lange (1995). A human telomeric protein. *Science 270*, 1663–1667.

d'Adda di Fagagna, F., M. P. Hande, W. M. Tong, D. Roth, P. M. Lansdorp, Z. Q. Wang, and S. P. Jackson (2001). Effects of DNA nonhomologous end-joining factors on telomere length and chromosomal stability in mammalian cells. *Curr Biol 11*, 1192–1196.

D'Amours, D. and S. P. Jackson (2002). The Mre11 complex : at the crossroads of dna repair and checkpoint signalling. *Nat Rev Mol Cell Biol 3*, 317–327.

de Lange, T. (2002). Protection of mammalian telomeres. *Oncogene 21*, 532–540.

de Lange, T. (2004). T-loops and the origin of telomeres. *Nat Rev Mol Cell Biol. 5*, 323–329.

de Lange, T. (2005). Shelterin: the protein complex that shapes and safeguards human telomeres. *Genes Dev 19*, 2100–2110.

de Lange, T. (2006). Lasker Laurels for telomerase. *Cell 126*, 1017–1020.

de Lange, T. and J. H. Petrini (2000). A new connection at human telomeres: association of the Mre11 complex with TRF2. *Cold Spring Harb Symp Quant Biol. 65*, 265–273.

Ducrest, A. L., H. Szutorisz, J. Lingner, and M. Nabholz (2002). Regulation of the human telomerase reverse transcriptase gene. *Oncogene 21*, 541–552.

Falck, J., J. Coates, and S. P. Jackson (2005). Conserved modes of recruitment of ATM, ATR and DNA-PKcs to sites of DNA damage. *Nature 434*, 605–611.

Foster, E. R. and J. A. Downs (2005). Histone H2A phosphorylation in DNA double-strand break repair. *FEBS J 272*, 3231–3240.

Gallego, M. E. and C. I. White (2001). RAD50 function is essential for telomere maintenance in Arabidopsis. *Proc Natl Acad Sci USA 98*, 1711–1716.

Greider, C. W. and E. H. Blackburn (1985). Identification of a specific telomere terminal transferase activity in Tetrahymena extracts. *Cell 43*, 405–413.

Greider, C. W. and E. H. Blackburn (1987). The telomere terminal transferase of Tetrahymena is a ribonucleoprotein enzyme with two kinds of primer specificity. *Cell 51*, 887–898.

Griffith, J., A. Bianchi, and T. de Lange (1998). TRF1 promotes parallel pairing of telomeric tracts in vitro. *J Mol Biol. 278*, 79–88.

Griffith, J. D., L. Comeau, S. Rosenfield, R. M. Stansel, A. Bianchi, H. Moss, and T. de Lange (1999). Mammalian telomeres end in a large duplex loop. *Cell. 97*, 503–514.

Hanahan, D. and R. A. Weinberg (2000). The hallmarks of cancer. *Cell 100*, 57–70.

Hockemeyer, D., A. J. Sfeir, J. W. Shay, W. E. Wright, and T. de Lange (2005). POT1 protects telomeres from a transient DNA damage response and determines how human chromosomes end. *EMBO J. 24*, 2667–2678.

Hopfner, K. P., A. Karcher, D. S. Shin, L. Craig, L. M. Arthur, J. P. Carney, and J. A. Tainer (2000). Structural biology of Rad50 ATPase: ATP-driven conformational control in DNA double-strand break repair and the ABC-ATPase superfamily. *Cell 101*, 789–800.

Hopfner, K. P. and J. A. Tainer (2003). Rad50/SMC proteins and ABC transporters: unifying concepts from high-resolution structures. *Curr Opin Struct Biol 13*, 249–255.

Horejsi, Z., J. Falck, C. J. Bakkenist, M. B. Kastan, J. Lukas, and J. Bartek (2004). Distinct functional domains of Nbs1 modulate the timing and magnitude of ATM activation after low doses of ionizing radiation. *Oncogene 23*, 3122–3127.

Houghtaling, B. R., L. Cuttonaro, W. Chang, and S. Smith (2004). A dynamic molecular link between the telomere length regulator TRF1 and the chromosome end protector TRF2. *Curr Biol. 14*, 1621–1631.

Jackson, S. P. (2002). Sensing and repairing DNA double-strand breaks. *Carcinogenesis 23*, 687–696.

Jacobs, J. J. and T. de Lange (2005). p16INK4a as a second effector of the telomere damage pathway. *Cell Cycle 4*, 1364–1368.

Jiang, W. Q., Z. H. Zhong, J. D. Henson, A. A. Neumann, A. C. Chang, and R. R. Reddel (2005). Suppression of alternative lengthening of telomeres by Sp100-mediated sequestration of MRE11/RAD50/NBS1 complex. *Mol Cell Biol 25*, 2708–2721.

Jimenez, G. S., F. Bryntesson, M. I. Torres-Arzayus, A. Priestley, M. Beeche, S. Saito, K. Sakaguchi, E. Appella, P. A. Jeggo, G. E. Taccioli, G. M. Wahl, and M. Hubank (1999). DNA-dependent protein kinase is not required for the p53-dependent response to DNA damage. *Nature 400*, 81–83.

Kanaar, R., J. H. Hoeijmakers, and D. C. van Gent (1998). Molecular mechanisms of DNA double strand break repair. *Trends Cell Biol. 8*, 483–489.

Karlseder, J., A. Smogorzewska, and T. de Lange (2002). Senescence induced by altered telomere state, not telomere loss. *Science. 295*, 2446–2449.

Karran, P. (2000). DNA double strand break repair in mammalian cells. *Curr Opin Genet Dev. 10*, 144–150.

Kim, S. H., P. Kaminker, and J. Campisi (1999). TIN2, a new regulator of telomere length in human cells. *Nat Genet. 23*, 405–412.

Kironmai, K. M. and K. Muniyappa (1997). Alteration of telomeric sequences and senescence caused by mutations in RAD50 of saccharomyces cerevisiae. *Genes Cells 2*, 443–455.

Kobayashi, J. (2004). Molecular mechanism of the recruitment of NBS1/hMRE11/hRAD50 complex to DNA double-strand breaks: NBS1 binds to gamma-H2AX through FHA/BRCT domain. *J Radiat Res 45*, 473–478.

Le, S., J. K. Moore, J. E. Haber, and C. W. Greider (1999). RAD50 and RAD51 define

two pathways that collaborate to maintain telomeres in the absence of telomerase. *Genetics 152*, 143–152.

Lee, J. H. and T. T. Paull (2004). Direct activation of the ATM protein kinase by the Mre11/Rad50/Nbs1 complex. *nce 304*, 93–96.

Lee, J. H. and T. T. Paull (2005). ATM activation by DNA double-strand breaks through the Mre11-Rad50-Nbs1 complex. *Science 308*, 551–554.

Lei, M., E. R. Podell, and T. R. Cech (2004). Structure of human POT1 bound to telomeric single-stranded DNA provides a model for chromosome end-protection. *Nat Struct Mol Biol. 11*, 1223–1229.

Li, B. and T. de Lange (2003). Rap1 affects the length and heterogeneity of human telomeres. *Mol Biol Cell 14*, 5060–5068.

Li, B., S. Oestreich, and T. de Lange (2000). Identification of human Rap1: implications for telomere evolution. *Cell 101*, 471–483.

Lim, D. S., S. T. Kim, B. Xu, R. S. Maser, J. Lin, J. H. Petrini, and M. B. Kastan (2000). ATM phosphorylates p95/nbs1 in an S-phase checkpoint pathway. *Nature 404*, 613–617.

Lisby, M. and R. Rothstein (2004). DNA repair: keeping it together. *Curr Biol Curr Bio*, R994–996.

Lisby, M. and R. Rothstein (2005). Localization of checkpoint and repair proteins in eukaryotes. *Biochimie 87*, 579–589.

Liu, D., M. S. O'Connor, J. Qin, and Z. Songyang (2004). Telosome, a mammalian telomere-associated complex formed by multiple telomeric proteins. *J Biol Chem. 279*, 51338–51342.

Loayza, D. and T. de Lange (2003). POT1 as a terminal transducer of TRF1 telomere length control. *Nature. 423*, 1013–1018.

Loayza, D. and T. de Lange (2004). Telomerase regulation at the telomere: a binary switch. *Cell. 117*, 279–280.

Maser, R. S. and R. A. Depinho (2002). Connecting chromosomes, crisis, and cancer. *Science 297*, 565–569.

Mirzoeva, O. K. and J. H. Petrini (2001). DNA damage-dependent nuclear dynamics of the Mre11 complex. *Mol Cell Biol 21*, 281–288.

Moncalian, G., B. Lengsfeld, V. Bhaskara, K. P. Hopfner, A. Karcher, E. Alden, J. A. Tainer, and T. T. Paull (2004). The rad50 signature motif: essential to ATP binding and biological function. *J Mol Biol 335*, 937–951.

Morales, M., J. W. Theunissen, C. F. Kim, R. Kitagawa, M. B. Kastan, and J. H. Petrini (2005). The Rad50S allele promotes ATM-dependent DNA damage responses and suppresses ATM deficiency: implications for the Mre11 complex as a DNA damage senso. *Genes Dev 19*, 3043–3054.

Moreno-Herrero, F., M. de Jager, N. H. Dekker, R. Kanaar, C. Wyman, and C. Dekker (2005). Mesoscale conformational changes in the DNA-repair complex Rad50/Mre11/Nbs1 upon binding DNA. *Nature 437*, 440–443.

Nugent, C. I., G. Bosco, L. O. Ross, S. K. Evans, A. P. Salinger, J. K. Moore, J. E. Haber, and V. Lundblad (1998). Telomere maintenance is dependent on activities required for end repair of double-strand breaks. *Curr Biol 8*, 657–660.

Paull, T. T. and M. Gellert (1998). The 3' to 5' exonuclease activity of Mre 11 facilitates repair of DNA double-strand breaks. *Mol Cell 1*, 969–979.

Paull, T. T. and M. Gellert (1999). Nbs1 potentiates ATP-driven DNA unwinding and endonuclease cleavage by the Mre11/Rad50 complex. *Genes Dev 13*, 1276–1288.

Paull, T. T., E. P. Rogakou, V. Yamazaki, C. U. Kirchgessner, M. Gellert, and W. M. Bonner (2001). A critical role for histone H2AX in recruitment of repair factors to nuclear foci after DNA damage. *Curr Biol 10*, 886–895.

Petrini, J. H. and T. H. Stracker (2003). The cellular response to DNA double-strand breaks: defining the sensors and mediators. *Trends Cell Biol 13*, 458–462.

Price, C. M. (1997). Synthesis of the telomeric C-strand. A review. *Biochemistry (Mosc) 62*, 1216–1223.

Ranganathan, V., W. F. Heine, D. N. Ciccone, K. L. Rudolph, X. Wu, S. Chang, H. Hai, I. M. Ahearn, D. M. Livingston, I. Resnick, F. Rosen, E. Seemanova, P. Jarolim, R. A. DePinho, and D. T. Weaver (2001). Rescue of a telomere length defect of Nijmegen breakage syndrome cells requires NBS and telomerase catalytic subunit. *Curr Biol. 11*, 962–966.

Shiloh, Y. (2003). ATM and related protein kinases: safeguarding genome integrity. *Nat Rev Cance 3*, 155–168.

Shore, D. (1994). RAP1: a protean regulator in yeast. *Trends Genet 10*, 408–412.

Slijepcevic, P. and S. Al-Wahiby (2005). Telomere biology: integrating chromosomal end protection with DNA damage response. *Chromosoma 114*, 275–285.

Smith, C. D., D. L. Smith, J. L. DeRisi, and E. H. Blackburn (2003). Telomeric protein distributions and remodeling through the cell cycle in Saccharomyces cerevisiae. *Mol Biol Cell 14*, 556–570.

Smogorzewska, A. and T. de Lange (2002). Different telomere damage signaling pathways in human and mouse cells. *EMBO J 21*, 4338–4348.

Smogorzewska, A. and T. de Lange (2004). Regulation of telomerase by telomeric proteins. *Annu Rev Biochem 73*, 177–208.

Smogorzewska, A., B. van Steensel, A. Bianchi, S. Oelmann, M. R. Schaefer, G. Schnapp, and T. de Lange (2000). Control of human telomere length by TRF1 and TRF2. *Mol Cell Biol. 20*, 1659–1668.

Stansel, R. M., T. de Lange, and J. D. Griffith (2001). T-loop assembly in vitro involves binding of TRF2 near the 3' telomeric overhang. *EMBO J. 20*, 5532–5540.

Stavridi, E. S. and T. D. Halazonetis (2005). Nbs1 moving up in the world. *Nat Cell Biol 7*, 648–650.

Stracker, T. H., D. V. Lee, C. T. Carson, F. D. Araujo, D. A. Ornelles, and M. D. Weitzman (2005). Serotype-specific reorganization of the Mre11 complex by adenoviral E4orf3 proteins. *J Virol. 79*, 6664–6673.

Stucki, M. and S. P. Jackson (2006). gammaH2AX and MDC1: anchoring the DNA-damage-response machinery to broken chromosomes. *DNA Repair (Amst) 5*, 534–543.

Su, T. T. (2006). Cellular Responses to DNA Damage: One Signal, Multiple Choices. *Annu Rev Genet 40*, 187–208.

Taggart, A. K., S. C. Teng, and V. A. Zakian (2002). Est1p as a cell cycle-regulated activator of telomere-bound telomerase. *Science 297*, 1023–1026.

Takai, H., A. Smogorzewska, and T. de Lange (2003). DNA damage foci at dysfunctional telomeres. *Curr Biol 13*, 1549–1556.

Usui, T., H. Ogawa, and J. H. Petrini (2001). A DNA damage response pathway controlled by Tel1 and the Mre11 complex. *Mol Cell. 7*, 1255–1266.

Usui, T., J. H. Petrini, and M. Morales (2006). Rad50S alleles of the Mre11 complex: questions answered and questions raised. *Exp Cell Res. 312*, 2694–2699.

Uziel, T., Y. Lerenthal, L. Moyal, Y. Andegeko, L. Mittelman, and Y. Shiloh (2003). Requirement of the MRN complex for ATM activation by DNA damage. *EMBO J 22*, 5612–5621.

van den Bosch, M., R. T. Bree, and N. F. Lowndes (2003). The MRN complex: coordinating and mediating the response to broken chromosomes. *EMBO Rep. 4*, 844–849.

van Steensel, B. and T. de Lange (1997). Control of telomere length by the human telomeric protein TRF1. *Nature. 385*, 740–743.

van Steensel, B., A. Smogorzewska, and T. de Lange (1998). TRF2 protects human telomeres from end-to-end fusions. *Cell 92*, 401–413.

Verdun, R. E., L. Crabbe, C. Haggblom, and J. Karlseder (2005). Functional human telomeres are recognized as DNA damage in G2 of the cell cycle. *Mol Cell 20*, 551–561.

Wang, R. C., A. Smogorzewska, and T. de Lange (2004). Homologous recombination generates T-loop-sized deletions at human telomeres. *Cell 119*, 355–368.

Wiltzius, J. J., M. Hohl, J. C. Fleming, and J. H. Petrini (2005). The Rad50 hook domain is a critical determinant of Mre11 complex functions. *Nat Struct Mol Biol 12*, 403–407.

Wright, W. E. and J. W. Shay (2000). Telomere dynamics in cancer progression and prevention: fundamental differences in human and mouse telomere biology. *Nat Med 6*, 849–851.

Wu, G., W. H. Lee, and P. L. Chen (2000). NBS1 and TRF1 colocalize at promyelocytic leukemia bodies during late S/G2 phases in immortalized telomerase-negative

cells: implication of NBS1 in alternative lengthening of telomeres. *J Biol Chem 275*, 30618–30622.

Yang, H., Q. Li, J. Fan, W. K. Holloman, and N. P. Pavletich (2005). The BRCA2 homologue Brh2 nucleates RAD51 filament formation at a dsDNA-ssDNA junction. *Nature. 433*, 653–657.

Ye, J. Z., J. R. Donigian, M. van Overbeek, D. Loayza, Y. Luo, A. N. Krutchinsky, B. T. Chait, and T. de Lange (2004). TIN2 binds TRF1 and TRF2 simultaneously and stabilizes the TRF2 complex on telomeres. *J Biol Chem. 279*, 47264–47271.

You, Z., C. Chahwan, J. Bailis, T. Hunter, and P. Russell (2005). ATM activation and its recruitment to damaged DNA require binding to the C terminus of Nbs1. *Mol Cell Biol 25*, 5363–5379.

Zhang, X. and T. T. Paull (2005). The Mre11/Rad50/Xrs2 complex and non-homologous end-joining of incompatible ends in *S. cerevisiae*. *DNA Repair (Amst) 4*, 1281–1294.

Zhang, Y., C. U. Lim, E. S. Williams, J. Zhou, Q. Zhang, M. H. Fox, S. M. Bailey, and H. L. Liber (2005). NBS1 knockdown by small interfering RNA increases ionizing radiation mutagenesis and telomere association in human cells. *Cancer Res 65*, 5544–5553.

Zhong, Z., L. Shiue, S. Kaplan, and T. de Lange (1992). A mammalian factor that binds telomeric TTAGGG repeats in vitro. *Mol Cell Biol 12*, 4834–4843.

Zhou, J., C. U. Lim, J. J. Li, L. Cai, and Y. Zhang (2006). The role of NBS1 in the modulation of PIKK family proteins ATM and ATR in the cellular response to DNA damage. *Cancer Lett 243*, 9–15.

Zhu, X. D., B. Kuster, M. Mann, J. H. Petrini, and T. de Lange (2000). Cell-cycle-regulated association of RAD50/MRE11/NBS1 with TRF2 and human telomeres.

Nat Genet. 25, 347–352.